Low-temperature thermochronologic insights into the exhumation of the northern Gawler Craton (South Australia)

Max Charles Reddy

November 2014

THE UNIVERSITY of ADELAIDE

LOW-TEMPERATURE THERMOCHRONOLOGIC INSIGHT INTO THE EXHUMATION OF THE NORTHERN GAWLER CRATON (SOUTH AUSTRALIA)

EXHUMATION OF THE NORTHERN GAWLER CRATON

ABSTRACT

The Gawler Craton (South Australia) records a complex thermal history during the Phanerozoic. Previous work has indicated that the central Gawler Craton was largely exhumed during the Carboniferous as a far-field effect of the Alice Springs Orogeny. Besides this widespread exhumation event, localised Mesozoic and Tertiary thermal events have been documented for the central Gawler Craton as well. The extent of these events into the northern Gawler Craton is not well understood as low-temperature thermochronological data is lacking for this region. For this study, granitoid samples along a roughly north-south transect through the northern and central Gawler Craton were analysed using the apatite fission track (AFT) and apatite (AHe) and zircon (ZHe) U-Th-Sm/He methods. Results from these low-temperature methods yield Neoproterozoic through to Cretaceous AFT, AHe and ZHe ages. Cumulative AFT age plots reveal a multi-phase Phanerozoic cooling history for the central and northern Gawler Craton. Significant AFT age peaks were found at ~480-450 Ma and ~350-300 Ma. The Ordovician age peak is thought to be related with the final stages of the Delamerian Orogeny, while the Carboniferous age peak is interpreted as being a far field response to the Alice Springs Orogeny. This is consistent with previous interpretations throughout South Australia. Additionally, localised Jurassic and Cretaceous AFT and ZHe ages were obtained which are thought to be related with rifting at the southern Australian margin and river incision respectively.

KEYWORDS

South Australia, northern Gawler Craton, Low-temperature Thermochronology, Apatite Fission Track, exhumation.

TABLE OF CONTENTS

LIST OF FIGURES AND TABLES

INTRODUCTION

The northern Gawler Craton has been recently intensively studied (Swain et al. 2005, Payne et al. 2006, Hand et al. 2007, Howard et al. 2011), its low-temperature thermal history, however, hasn`t yet been systematically investigated. Few recent apatite fission track (AFT) studies have been carried out within the central Gawler Craton (Gleadow et al. 2002, Kohn et al. 2002, Boone 2013) with two main low-T thermal events being identified for the region. (1) an older cooling event during the Carboniferous (335.3±2.0 Ma) (Gleadow et al. 2002, Kohn et al. 2002) and (2) a younger thermal event during the Eocene (41.4 ± 1.6 Ma) (Gleadow et al. 2002, Kohn et al. 2002). The Carboniferous cooling episode has also been reported for the Flinders Ranges (commencing at c. 360-300 Ma) and is thought to represent a period of regional exhumation within South Australia as a far field response to the Alice Springs Orogeny. (Mitchell et al. 1998, Gibson and Stüwe 2000, Tingate and Duddy 2002, Tingate et al. 2007). Studies in surrounding regions such as the Flinders Ranges and Adelaide Hills have also recognised younger thermal event(s) represented by a number of late Cretaceous-Tertiary AFT ages or cooling episodes (Mitchell et al. 1998, Gibson and Stüwe 2000, Tingate and Duddy 2002, Tingate et al. 2007). The younger AFT ages produced in these studies are widely interpreted as the result of a widespread Late Cretaceous exhumation event across south central Australia (Macdonald et al. 2013).

AFT constraints on the low-temperature thermal history of the northern Gawler Craton are currently lacking. This thesis aims to resolve the low temperature thermal history of the northern Gawler Craton by applying a suite of thermochronometric methods (apatite fission track (AFT) dating, zircon U-Th-Sm/He (ZHe) dating and apatite U-Th-Sm/He

(AHe) dating) and to test if the northern Gawler Craton was also affected by these two regional thermal events.

In this paper, I present low-temperature thermochronometric data from a series of igneous rock samples within the northern and central Gawler Craton. Samples were taken along a roughly north-south trending profile over the entire northern and central Gawler Craton which allows evaluation of the extent of aforementioned thermal events on a regional scale. Resulting AFT, ZHe and AHe data were modelled to provide a complete reconstruction of the low-temperature thermal history of the study region throughout the Phanerozoic. In this thermal history model, important cooling phases are identified and their tectonic significance is discussed.

GEOLOGICAL SETTING/BACKGROUND

Pre-Phanerozoic tectonic history of the Gawler Craton

The Gawler Craton consists largely of crystalline basement which extends throughout central South Australia covering an area of approximately 480,000km² (Fanning et al. 1988). The craton encompasses the area north of Tarcoola and Coober Pedy and reaches as far south as the north coast of Kangaroo Island (Figure 1). It is composed of Late Archean to Mesoproterozoic granites, volcanics and metasediments (Fanning et al. 1988).

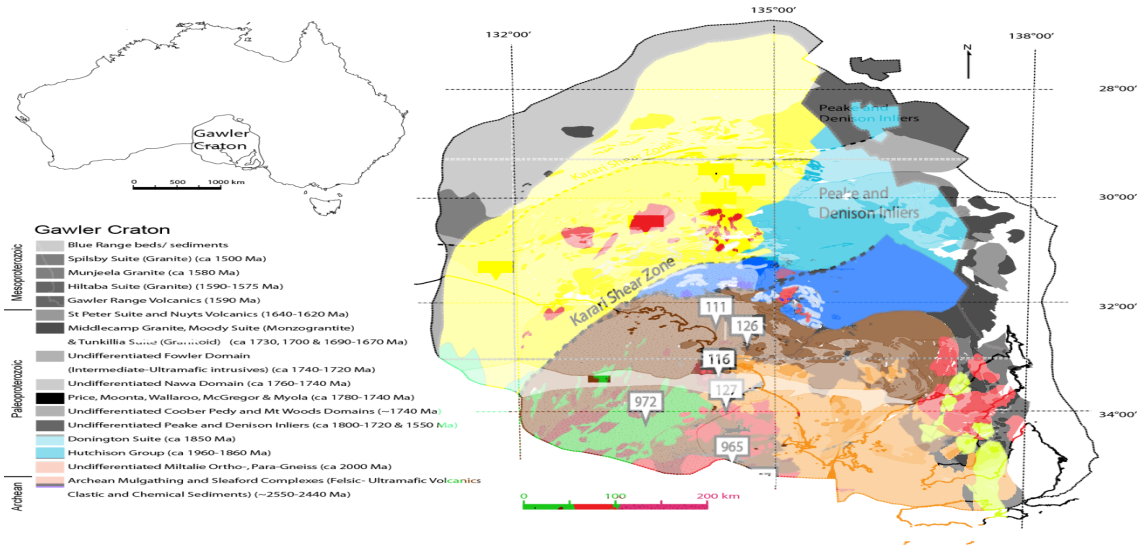

Figure 1: Simplified geological map of the Gawler Craton, modified from Howard et al. (2011). Sample locations for this study are indicated by their sample numbers on the map. As shown, a roughly north-south profile was sampled mainly targeting granitoids in the northern and central Gawler Craton. One additional sample (952) comes from a drill core in the Eucla basin.

The Gawler Craton is regarded as being a tectonically stable platform since 1450 Ma, and has experienced tectonic quiescence since the early Palaeozoic (Webb et al. 1986, Fanning et al. 1988). Prior to this, several major crustal formation and tectonothermal events occurred throughout the Gawler Craton during the interval 3200-1500 Ma which are described as the Sleaford Orogeny (2480-2420 Ma) and the Kimban Orogeny (1730-1690 Ma) (Hand et al. 2007). These events are summarised in Table 1.

Table 1: Adapted from Hand et al. (2007) detailing the major tectonothermal events to affect the Gawler Craton and their characteristics.

Event	Distribution within the Gawler Craton	Age Range (Ma)	Metamorphic style	Magmatism
Sleafordian Orogeny	Entire proto-craton	2480-2420	High heat flow, low to moderate P	Felsic
Miltalie Event	Eastern craton	Approx 2000	Unknown	Unknown
Cornian Orogeny	Eastern craton	1855-1845	High heat flow, moderate P	Felsic, minor mafic: large volume
Kimban Orogeny	Entire craton	1730-1690	High to low heat flow	Felsic and Mafic: large volume
Ooldean Event	Western craton	1660-1630	High heat flow, low P	Felsic
Deformation Associated with St Peter Suite	Southwestern craton	1620-1610	High heat flow	Felsic and Mafic
Deformation Associated with Hiltaba Suite	Entire craton	1595-1575	High heat flow	Felsic and Mafic: large volume
Kararan Orogeny	North and western craton	1570-1540	Moderate heat flow	None Known
Coorabie Orogeny	Western craton	1470-1450	Moderate heat flow	None Known

Following the late Palaeoproterozoic Kimban Orogeny, the emplacement of extensive magmatic rock suites was the main control on tectonic development within the craton (Hand et al. 2007). These include the Gawler Range Volcanics (c. 1595-1575 Ma) along with the comagmatic Hiltaba Suite intrusives (c. 1595-1575 Ma). During the late Palaeoproterozoic – early Neoproterozoic (1700-900 Ma), the North Australian Craton, the West Australian Craton and the Gawler Craton amalgamated together which formed the basis for the Australian continent (Gale 1992).

Phanerozoic tectonic history of the Gawler Craton

Several major Phanerozoic tectothermal events affected southern Australia which are summarised in Table 2. The Gondwana supercontinent formed during the time period

(650-550 Ma) which resulted in a period of relative tectonic stability within the Gawler Craton prior to development of the Southern Ocean Rift during the Jurassic (Gale 1992). Regionally, the latest Proterozoic to early Cambrian Petermann Orogeny (600-530 Ma) was the first of two major intracratonic orogenic events that shaped the crustal architecture of central Australia (Sandiford and Hand 1998, Raimondo et al. 2014), the second being the Alice Springs Orogeny. These events were largely caused by far-field propagation of plate boundary derived stresses into the continental interior (Raimondo et al. 2014). The extent of these central Australian orogens is not clear due to a lack of exposure (Raimondo et al. 2014), and as a result the effect they had on the Gawler Craton is not well studied. Geochronological, geophysical and sedimentological evidence suggests that they are similarly extensive and that the tectonic activity attributed to these events across Australia indicate continent scale impact (Raimondo et al. 2014).

The Cambro-Ordovician Delamerian Orogeny had a major effect on the southern Australia basement as well. Initiated in the present day Adelaide Fold Belt during the Cambrian (514±3 Ma) (Foden. et al. 2006), contractional (eastward propagating) orogenisis occurred until 490±3 Ma. The final phase of the Delamarian Orogeny induced rapid uplift, cooling and exhumation, accompanied by post-tectonic magmatism.(Foden. et al. 2006). The orogeny extended at least as far north as the Peake and Denison Inliers to the northeast of the study area (Drexel and Preiss 1995). Gibson and Stüwe (2000) identified a localised thermal event within the Mount Lofty Ranges and Murray Bridge areas of the Adelaide Fold Belt prior to 350Ma. They suggested that this thermal event could be related to exhumation associated with the latest stages of

inversion during the Delamerian Orogeny. No other low-temperature thermochronological data has been reported for this time period in South Australia as the thermal history is likely overprinted by subsequent tectonic and thermal events. The effects of the Delamerian Orogeny on the study area of this thesis are thus not well studied.

The Devonian to Carboniferous Alice Springs Orogeny (450-300 Ma) was the second major intraplate event that affected central Australia following the Petermann Orogeny (Raimondo et al. 2014). Previous low-temperature thermochronological studies by (Tingate and Duddy 2002) within the eastern Officer Basin and the studies by Gibson and Stüwe (2000) and Mitchell et al. (1998) within the Adelaide Fold Belt report apatite fission track cooling ages between 360-300 Ma. It was interpreted that these older cooling histories were most likely related to the Alice Spring Orogeny (370-300 Ma). AFT Studies by Gleadow et al. (2002), Kohn et al. (2002) and unpublished work by Boone (2013) within the Gawler Craton record similar AFT ages indicating that the Alice Springs Orogeny may have affected central and southern Australia on a regional scale. Cumulative results from these studies have produced a well-defined AFT age peak that is centred within the Carboniferous (327.4±1.8 Ma) indicating that regional cooling occurred during the final phases of the Alice Springs Orogeny. Alternatively, recently obtained time-temperature models indicate that the central Gawler Craton underwent slow cooling throughout the Palaeozoic before stabilizing at near surface temperatures (~20-40˚C) until present day (Boone 2013). Hence, these models show no clear evidence for increased cooling in the central Gawler Craton during the Alice Springs Orogeny but indicate long lasting, slow exhumation of the Gawler Craton

(Boone 2013). These cooling patterns are typical of Australian cratons and are thought to represent prolonged exhumation of cratonic shield areas (Boone 2013).

The beginning of the Jurassic is marked by the development of the Southern Ocean Rift that resulted from the breakup of eastern Gondwana (Veevers et al. 1991, Drexel and Preiss 1995). Onset of sea floor spreading occurred in the late Jurassic (~160 Ma). This resulted in large scale transport of sediments throughout Eastern Australia via rivers from the Tasman Divide, close to the modern day east coast of Australia (Gurnis 1998). The Great Artesian Basin formed as a result of this process. This rifting continued through the Cretaceous. Spreading rates increased during the Tertiary and by the middle Eocene Australia and Antarctica had completely separated (Etheridge et al. 1991, Kohn et al. 2002). This process induced large scale surface denudation within southern Australia that began at ~43 Ma (Sandiford 2007).

Table 2: Major Phanerozoic tectonothermal events to affect southern Australia.

Event	Extent	Age Range (Ma)
Petermann Orogeny	Probably continent scale.	~600-500
Delamerian Orogeny	At least as far south as Kangaroo Island and as far north as the Peake and Denison Inliers. Narrow east-west extent.	~514-490
Alice Springs Orogeny	Probably continent scale.	~450-300
Southern Ocean Rift Development	Entire southern Margin of Australia.	~200-40

Abundant and widespread AFT data reported by (Macdonald et al. 2013) indicate that the Meso-Cenozoic processes at the plate margins may have induced cooling and exhumation accross southern and central South Australia. Boone (2013) suggested that

Mesozoic-Cenozoic cooling and exhumation is mainly a result of the initiation of fast spreading in the Southern Ocean and the subsequent northward tilting of the Australian continent.

During the Mesozoic, a reheating event induced by burial and associated hydrothermal activity is interpreted to have occurred in the northern Flinders Ranges (Weisheit et al. 2014). This was based on Mesozoic AFT ages (Mitchell et al. 2002). AFT data reveals a similar reheating event within the central Gawler Craton that occurred during the Cretaceous-Tertiary (Gleadow et al. 2002, Kohn et al. 2002). Kohn et al. (2002) speculated that this reheating event was related directly to the Jurassic- Paleogene Eromanga Basin System through either burial by sedimentary cover or heat transfer via hydrothermal fluids. The youngest AFT ages within South Australia (32-25 Ma) were produced in the Paralana Fault zone and surrounding country rock in the nearby Flinders Ranges (Foster et al. 1994). These Oligocene AFT ages are thought to be a result of hydrothermal activity within the Eromanga Basin.

Sedimentology of major basins in the vicinity of the study region

The following section gives a brief overview of the sedimentary record of the major basins in the vicinity of the study area in the northern Gawler Craton. These sediments often represent the erosion products of the exhumed basement inliers which provide independent constraints on the exhumation history of the Gawler Craton. Information on sedimentary formations within the study area is presented in Table 3.

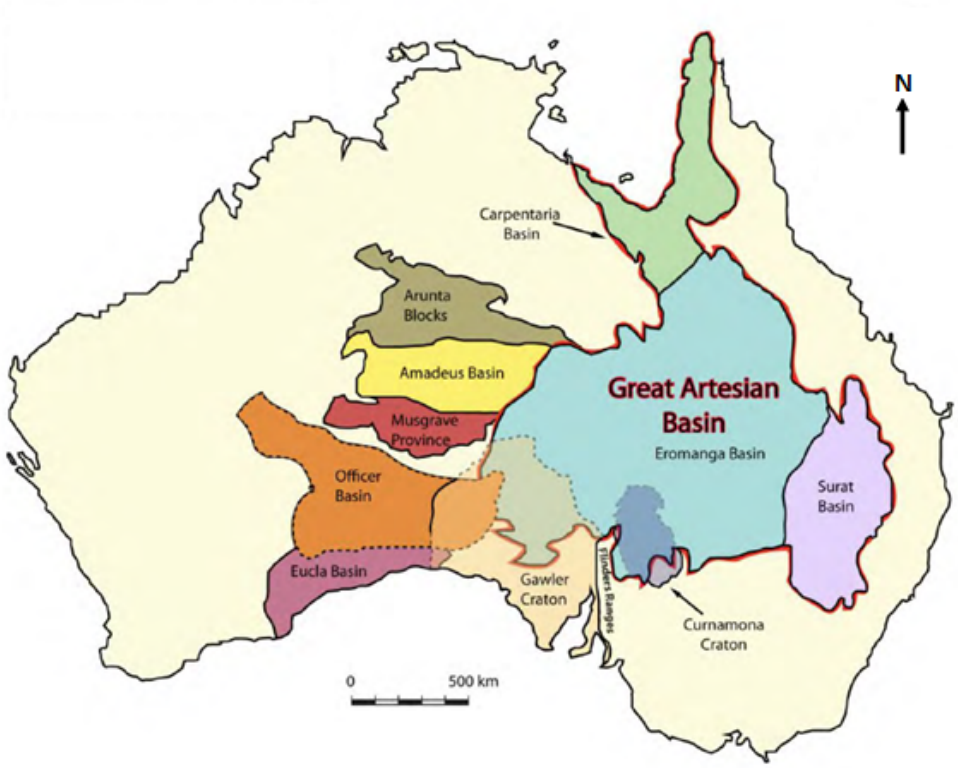

Figure 2: Regional Map of Australia showing the location of significant Basins and Cratons, adapted from (Boone 2013).

The Neoproterozoic to mid- Palaeozoic Officer Basin extends eastwards from central Western Australia into South Australia, the eastern Officer Basin is characterised by shallow marine and fluvial sediments and is unconformably overlain by thin Permian sediments of the Arckaringa Basin, Cretaceous sediments of the Eromanga Basin and Tertiary successions (Tingate and Duddy 2002). To the southeast, compressional deformation associated with the Alice Springs Orogeny has been documented (Drexel and Preiss 1995).

Table 3: Description of the major sedimentary formations to exist in this study area from. From (Drexel and Preiss 1995, Alexander and Hibburt 1996, (PIRSA) 2009, Geoscience-Australia 2014).

Basin	Formation	Age Range (Ma)	Lithology(s)	Predominant Depositional Environment(s)
Officer Basin	Observatory Hill Formation	Early-middle Cambrian	Sandstone, Siltstone, Shale, Mudstone, Limestone	Shallow marine (carbonate rich sections), Fluvial
Arckaringa Basin	Boorthanna Formation	Early Permian	Diamictite, Coarse to fine grained clastics	Marine, Fluvio-glacial
	Stuart Range Formation	Early Permian	Shale, minor Siltstone and Sandstone	Shallow Marine (quiet water restricted)
	Mount Toondina	Early Permian	Silstone, Sandstone. Coal, Shale and minor Carbonate interbeds	Marine, Lacustrine at base, Deltaic to Lacustrine and Fluvial towards top of formation
Eromanga Basin	Algebuckina Sandstone	Jurassic-Lower Cretaceous	Sandstone (fine to coarse)	Fluvial, Lacustrine, Alluvial
	Cadna-owie Formation	Lower Cretaceous	Sandstone, Siltstone	Terrestrial to Marine transition
	Bulldog Shale	Lower Cretaceous	Shale, Mudstone, minor Siltstone and Sandstone	Marine
Eucala Basin	Garford Formation	Miocene-Pliocene	Mudstone, Carbonate, minor Sandstone	Lacustrine
	Pidinga Formation	Eocene	Sandstone, Siltstone, Mudstone	Fluvial, Estuarine

The Permian Arckaringa Basin covers 80,000 km² within South Australia. It consists of three main formations, the Boorthanna Formation, Stuart Range Formation and the Mount Toondina Formation (Drexel and Preiss 1995). These formations contain marine, shallow marine, glacial, deltaic, fluvial and lacustrine sediments.

The Jurassic-Cretaceous Eromanga Basin consists of three major formations. These are the Algebuckina Sandstone, the Cadna-owie Formation and the Bulldog Shale. These contain marine, lacustrine, fluvial and alluvial sediments. The Cenozoic Eucala Basin extends in to the far southwest of the study area. It is an onshore-offshore basin covering parts of Western Australia, South Australia and into the Great Australia Basin. Eucala Basin Tertiary sediments are only sporadically observed in the study area. These are predominantly within the Pidinga and Garford Formations.

SAMPLES AND METHODOLOGY

Apatite fission-track thermochronology

Apatite Fission Track low-T Thermochronology is based on the spontaneous fission decay of ^{238}U that produces damage trails (fission tracks) within the crystal lattice (Wagner and Van den Haute 1992, Tagami and O'Sullivan 2005). These fission tracks are thermally unstable and not preserved at elevated temperatures (Green et al. 1986). Therefore the AFT chronometer dates the time when fission tracks become thermally stable. The temperature at which tracks are no longer preserved is termed the closure temperature (Green et al. 1986). The closure temperatures is dependent on the chemical composition of apatite, in particular the Cl/F ratio (O'Sullivan and Parrish 1995), however, it is typically between 125-100°C (Wagner and Van den Haute 1992). At

temperatures below the closure temperature (but above ~60°C) tracks are shortened or annealed (Wagner and Van den Haute 1992). This temperature range is called the partial annealing zone (PAZ). Below ~60°C, the tracks are believed to be stable. An AFT age can be calculated for a given sample by obtaining a spontaneous fission track density and a measured 238-Uranium concentration. This AFT age generally represents the timing of cooling though the PAZ. Mean confined track lengths provide additional information on the rate of cooling through the PAZ (Green et al. 1986). Fission track age and length data can subsequently be modelled to produce a time-temperature model for the thermal history of the study region (Tagami and O'Sullivan 2005). For a more detailed description of AFT thermochronology theory refer to (Green et al. 1986, Wagner and Van den Haute 1992, Tagami and O'Sullivan 2005). Sample details including locations, lithology and applied methodologies are listed in Table 4.

Table 4: Sample location, lithology, source and applied methods details. RO = rock outcrop, DC = drill core, AFT = Apatite Fission Track, AHe = U-Th-Sm/He, ZHe = U-Th-Sm/He.

Sample	Latitude	Longitude	Altitude (m)	Lithology	Stratigraphic Unit	Formation Age (Ma)	Source	Methods Applied
111	-29.5934	134.3550	152	Granite	Hiltaba Suite	1590-1575	RO	AFT ZHe
116	-30.0318	134.3451	154	Gneiss	Mulgathing Complex	Archean	RO	AFT
126	-29.7322	134.7057	163	Rhyodacite	Gawler Range Volcanics	1590	RO	AFT
127	-30.3405	134.5218	145	Microgranite	Hiltaba Suite	1590-1575	RO	AFT
952	-31.3528	131.8547	50	Gabbro	Unknown	Unknown	DC	AFT AHe
965	-31.0582	134.5313	146	Granite	Tunkillia Suite	1690-1670	RO	AFT
967	-31.3085	134.8369	135	Granite	Tunkillia Suite	1690-1670	RO	AFT
972	-30.5509	133.5415	161	Granite	Wynbring Granite	1701 ± 30	RO	AFT, AHe, ZHe

Samples 952, 965, 967 and 972 were received as apatite separates. Samples 111, 116, 126 and 127 were received as whole rock samples that were crushed and separated

using conventional magnetic and heavy liquid techniques. Apatite grains from each sample were arranged in rasters onto glass slides using Olympus SZ61 microscopes at 45x magnification and then mounted using epoxy resin. Samples were ground and polished to reveal an internal surface and subsequently etched in 5 mol/L HNO_3 at 20˚C for 20 seconds to reveal fission tracks. Fission tracks were counted using an Olympus BX51 microscope at 1000x magnification. Confined track lengths were measured using an accompanying Olympus BX51 digital camera and handset connected to a computer. An international standard apatite (Durango apatite) and an in-house standard (ARK 707 – Arkaroola) were counted for calibration purposes. The sample uranium content was measured using Laser Ablation-Inductively Coupled Plasma-Mass Spectrometry (LA-ICP-MS) as opposed to conventional thermal neutron irradiation (Hasebe et al. 2004, De Grave et al. 2012). Data reduction procedures and AFT age calculations were carried out using an in-house MS Excel® spreadsheet provided by Dr. Stijn Glorie (The University of Adelaide), based on the protocols outlined in (Hasebe et al. 2004). Individual and Cumulative Radial Plots were created for all samples using the software program RadialPlotter (Vermeesch 2009). The automatic mixture model of RadialPlotter was used to identify statistical AFT age peaks within samples. Dpar (etch bit) measurements were taken from all apatite grains that were counted. These Dpar data are measures of the individual apatite annealing kinetics (linked with the apatite chemistry) and provide an independent control on the age-peak identification process. Lastly, thermal histories were modelled using the software program HeFTy which uses forward and inverse modelling (Ketcham 2005). For a more detailed description of the AFT methodology see appendices.

Apatite and Zircon (U-Th-Sm)/He thermochronology

Apatite (AHe) and Zircon (ZHe) U-Th-Sm/He low-T thermochronology is based on the temperature-dependant diffusivity of radiogenic ^{4}He through the crystal lattice. For apatite, this method records the time of cooling below ~45-75˚C (Ehlers and Farley 2003). The ZHe method records cooling at much higher temperatures of ~200-180˚ C (Wolfe and Stockli 2010). Both the AHe and ZHe dating methods are widely used in conjunction with the AFT technique in refining time-temperature models (Ehlers and Farley 2003).

Selected apatite and zircon separates were sent for U-Th-Sm/He analysis at the John de Laeter Centre for Isotope Research, Curtin University. 10-15 apatite and 8-10 zircon grains were selected for each sample based on crystal quality (e.g. euhedral crystals, inclusion-free). The analysis involved thermal extraction of helium using a 1064 nm Nd-YAG laser that a ^{4}He abundances to be determined via an Agilent 7500CS mass spectrometer. U and Th contents were determined using isotope dilution inductively coupled mass spectrometry via the Agilent 7500CS mass spectrometer. For a more detailed description of the apatite and zircon U-Th-Sm/He thermochronology methodology (see appendices).

OBSERVATIONS AND RESULTS

Apatite Fission Track calibration

Two standards were used for calibration purposes and accuracy check of the obtained results. These are the international standard apatite (Durango apatite) and an in-house standard (ARK 717 – Arkaroola). The results obtained for both standards are presented

in Figures 3 and 4. The radial plot of international standard Durango apatite is comprised of ages calculated in this study, based on multi-grain data obtained via LA-ICP-MS. The central age value is calculated as 32±1.5 Ma which is within error to the precisely obtained ^{40}Ar–^{39}Ar reference ages of 31.44±18 (McDowell et al. 2005), which validates the accuracy of the results obtained for this study.

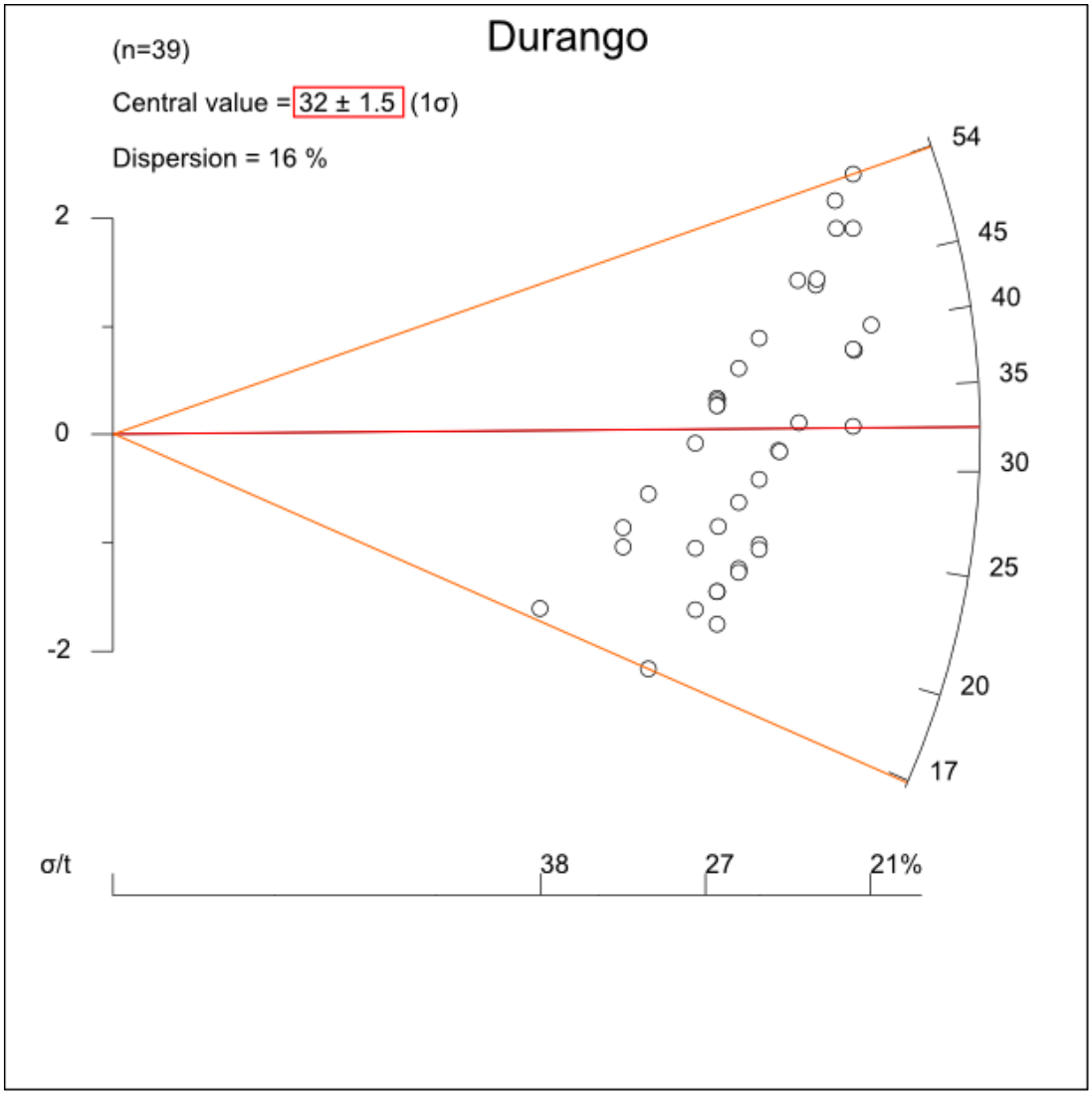

Figure 3: Radial plot for Durango apatite age calculations used as the international standard in this study. The plot was made using RadialPlotter (Vermeesch 2009). Each point represents the age obtained for individual grains. The age for each grain on the plot is obtained by projecting a line from the origin, through an individual point and to the curved age axis in Ma. The scale on the left shows the standard deviation of the dataset. The further a point plots to the right, the more precise the measurement is, demonstrated by the horizontal precision axis below the plot. For this plot, a central age of 32±1.5 Ma (red line) with a dispersion of 16% was obtained, n represents the number of grains analysed. The maximum and minimum grain ages are highlighted by the two orange lines.

A secondary accuracy check was performed using an in-house standard (ARK 717). Figure 4 compares the results obtained for this study (Plot 3) with those obtained by Hons candidate Mr. Jack Gillespie (Plot 2) and unpublished data by Dr. Stijn Glorie for sample TTN1 (Plot 1) which was taken in close proximity to sample ARK717. Latter data was obtained using the classical AFT method which involves neutron irradiation instead of direct ^{238}U measurements. As shown, the results obtained in this thesis are comparable to those obtained by previous researchers (Plot 1 & 2). The comparison with the data for TTN1 (plot 1) validates the applied method protocol, while the comparison with plot 2 illustrates internal consistency.

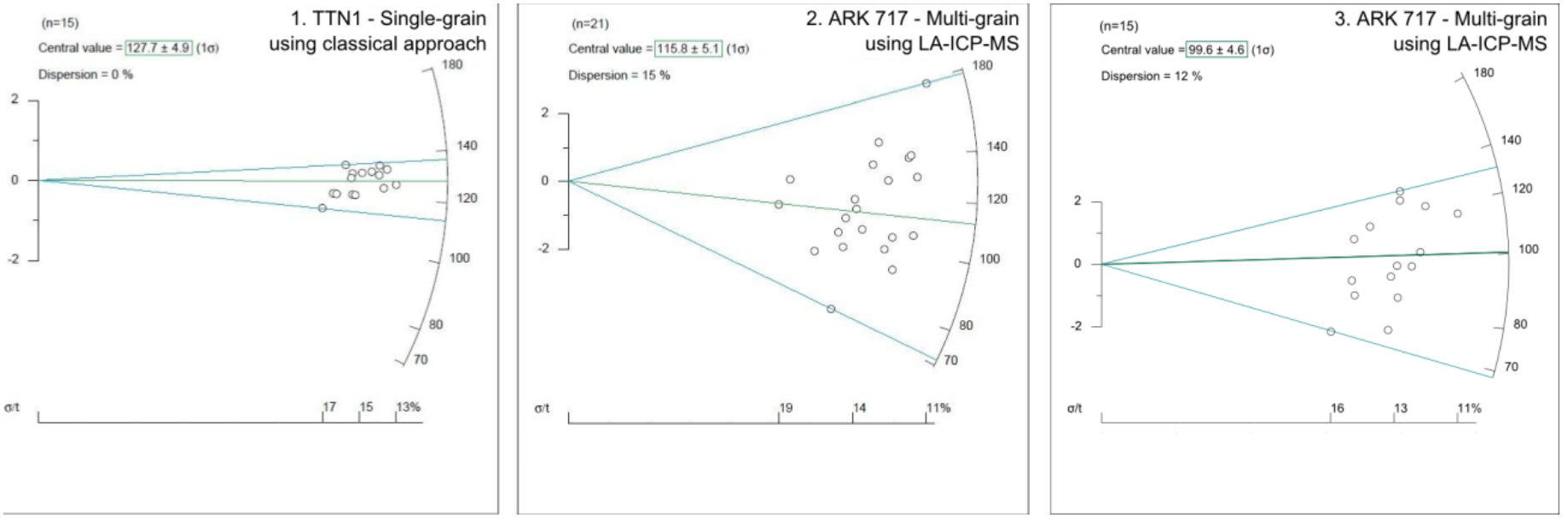

Figure 4: Radial plots showing data obtained for in-house standards from Arkaroola, South Australia. Plots 1 and 2 display data obtained by Dr. Stijn Glorie and Mr. Jack Gillespie respectively. The ARK 717 (UTM coordinates 54J 341962 / 6657785) (image 2 & 3) plot is based on multi-grain data obtained via LA-ICP-MS. The comparable results between image 2 and 3 demonstrate internal consistency. TTN1 (image 1) is located in close proximity to ARK 717 and is based on single-grain data obtained via the classical AFT method (which explains the tighter clustering of the individual data points for TTN1). Comparable results between samples TTN1 and ARK 717 demonstrate the validity of the LA-ICP-MS method. For TTN1 sample details refer to (Weisheit et al. 2014). ARK 717 is an in-house standard with an identical exhumation history to TTN1. Radial plots produced using RadialPlotter software (Vermeesch 2009). See Figure 3 for a description on radial plots.

Apatite Fission Track results

Apatite Fission Track analysis was carried out on 13 Samples in the northern Gawler Craton and surrounds. Results from AFT dating and length measurements are summarised in Figures 5 and 6 and Table 5. AFT age peaks were calculated using the automatic mixture model in RadialPlotter.

For sample 952 which was taken in the southwest of the study region (drill core at the margin of the Eucla Basin, Figure 1 & 5), two AFT age peaks were obtained, a Cambrian (521±20 Ma) age and an early Carboniferous (358±17 Ma) age (Figure 6). This is suggestive of a Carboniferous cooling event, while an older Cambrian event is partially preserved. The length histogram for this sample is bimodal with a large standard deviation of 2.38μm reflecting multiple cooling and reheating events which are accommodated by the multiple AFT age peaks.

Sample 972 which was taken from the central Gawler Craton, yields two AFT age peaks, an early Cambrian (532±44 Ma) age and a Permian (278±16 Ma) age (Figure 6). The statistically acceptable minimum AFT age obtained for this sample is Triassic (226±39 Ma). Length data appears to produce a unimodal distribution with an average confined track length of 11.33μm. This suggests that this sample underwent considerably slow cooling through the PAZ sometime between the Permian and Triassic.

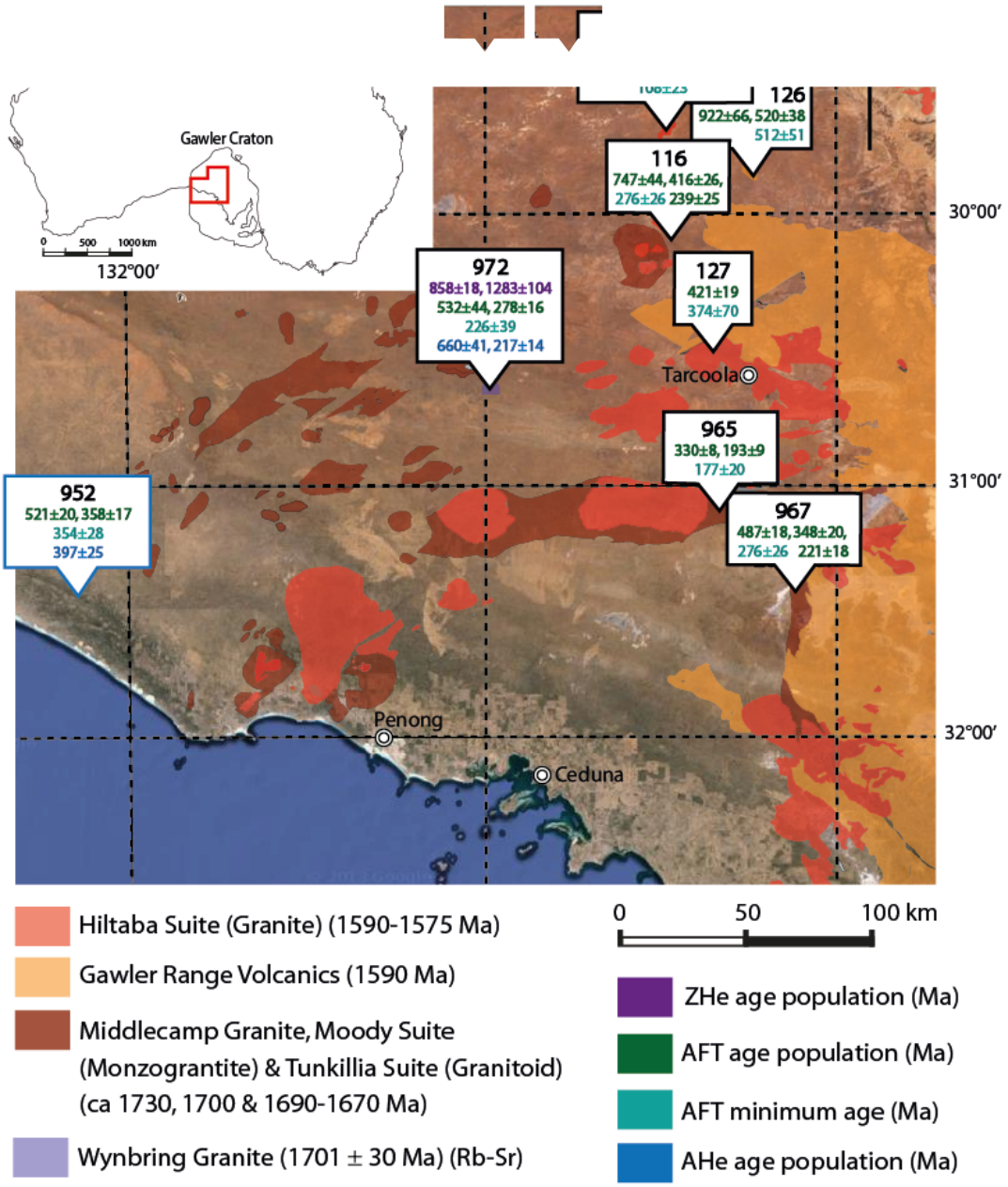

Figure 5: Simplified geological map overlying a Google Earth satellite image. Modified from Howard et al. (2011). Major intrusions and sample locations are shown. Sample 952 is outlined in blue because it is from drill core as opposed to rock outcrop. ZHe age peaks are in purple font, AFT age peaks in dark green and AHe age peaks in blue. AFT minimum ages are in aqua font. All ages are in Ma.

In the southeast of the study region, sample 967 records three AFT age peaks, a late Cambrian (487±18 Ma), an early Carboniferous (348±20 Ma) and a Triassic (221±18 Ma) age (Figure 6). The youngest Triassic age peak is constrained by two single grains only and caution is required to not interpret this age in too much detail. The minimum statistical acceptable age-component for the entire data-set is constrained to the Permian (276±26 Ma). Confine track lengths for this sample are unimodal in distribution with an average length of 12.28µm. These results are indicative of moderate cooling rates. Nearby, sample 965 yields two AFT age peaks, a Carboniferous (330±8 Ma) age and an early Jurassic (193±9 Ma) age (Figure 6). The minimum AFT age is Jurassic (177±20 Ma) which confirms that cooling occurred at least until the Jurassic. Confined track length data for this sample is unimodal with an average length of 13.20µm which is indicative of fast cooling rates.

Further north, sample 127 yields one single AFT age peak which is late Silurian (421±19 Ma) in age (Figure 6). The minimum age for this sample is Devonian (374±70 Ma). This is indicative of Silurian-Devonian cooling. Sample 116 yields three AFT age peaks, a Neoproterozoic (747±44 Ma) age, an early Devonian (416±26 Ma) and a Triassic (239±25 Ma) age (Figure 6). The Neoproterozoic age is poorly constrained by three grains only. The minimum AFT age is Triassic (223±28 Ma) which validates the youngest obtained age component. Fission track length data could not be obtained for this sample due to insufficient confined fission tracks in the apatite grains.

Sample 126 yields two AFT age peaks, a Neoproterozoic (922±66 Ma) age and a Cambrian (520±38 Ma) age (Figure 6). The minimum AFT age is Cambrian (512±51

Ma) and thus mimics the youngest component. These ages suggest that this sample most recently underwent cooling through the PAZ during the Cambrian which is significantly older than for the surrounding samples.

In the northern end of the study area, sample 111 yields two AFT age peaks. These are a late Permian (258±38 Ma) and a Cretaceous (133±7 Ma) age (Figure 6). The minimum AFT age is (108±23 Ma). This suggests that this sample underwent cooling to near surface conditions during the Cretaceous, much more recently than all other samples.

Dpar measurements for all grains analysed in this study are represented by the red-yellow colour scheme on the radial plots (Figure 6). Patterns between the Dpar measurements (reflecting apatite chemistry) and the single grain ages are generally weak throughout all samples. The decomposition of the data-sets in multiple age components is thus generally unsupported by the obtained Dpar data.

Figure 6: (next page). Radial plots of all samples in this study displaying all low-T data obtained in this study, as well as length histograms where available. Radial plots were constructed using the software program RadialPlotter (Vermeesch 2009). See Figure 3 for a description on radial plots. AFT age peaks are presented as green lines on the plot, ZHe age peaks in purple, AHe age peaks in blue and AFT minimum age peaks in teal. AFT age peaks and statistically acceptable minimum AFT ages were calculated using the automatic mixture model in RadialPlotter. Peak ages are listed alongside peak lines within the plot. For each AFT age peak, the percentage of data used to constrain the peak is given between brackets plus or minus the dispersion for that AFT age peak. The colour given to each point on the plot indicates the average of five Dpar measurements taken from that grain which is a measure for the apatite chemistry. The red-yellow colour bar below each plot shows the colour scheme that Dpar lengths can be obtained by, given in micrometres. Length data is presented as histograms, lm is the average confined track length, n is the number of confined tracks identified and measured and σc is the standard deviation of confine track lengths.

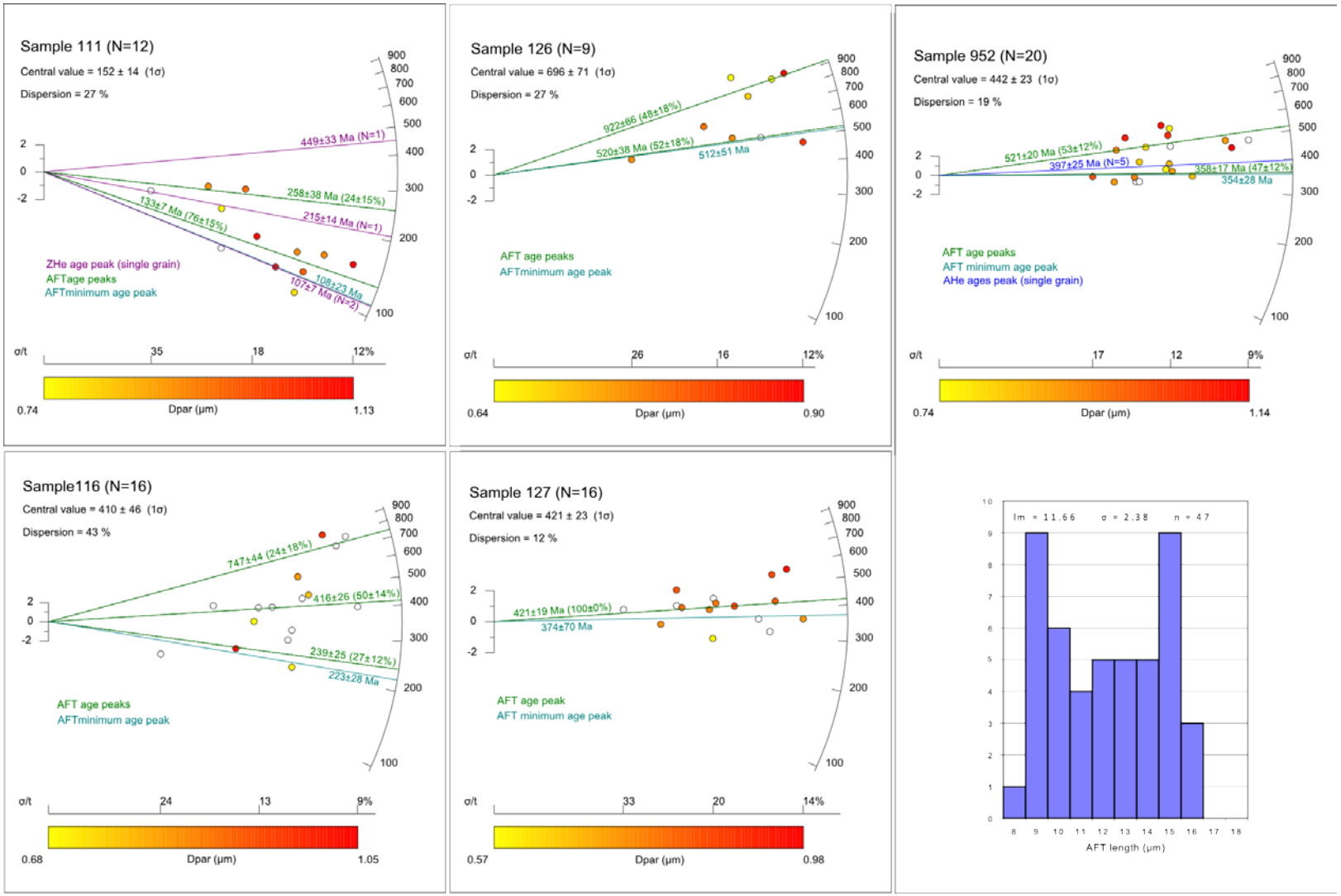

Figure 6: For description see above.

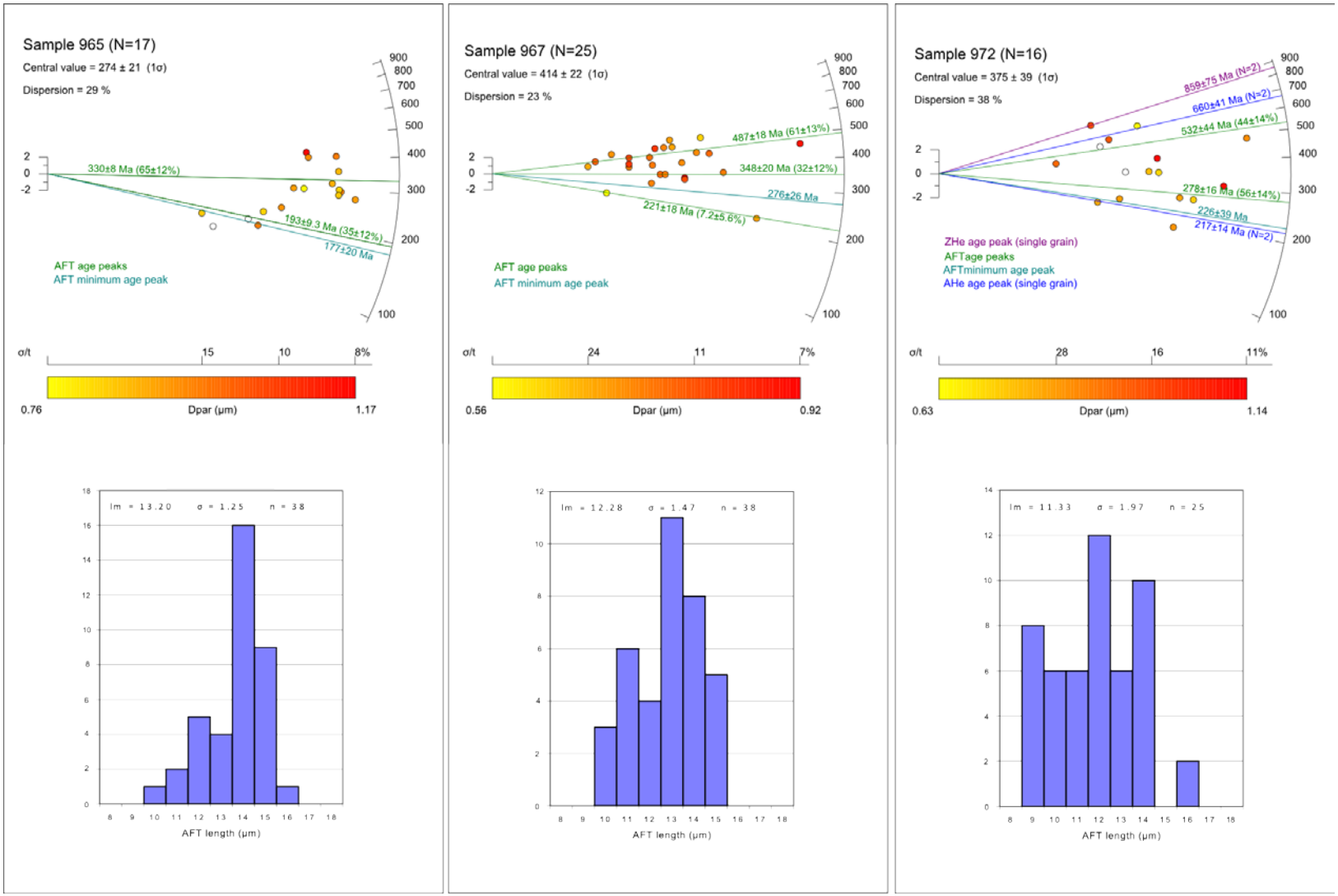

Figure 6: (continued)

Table 5: AFT results for all samples in this study including confined track length data. Results of individual age peaks within samples are included. ρ_s is the surface density of spontaneous fission tracks (in 10^5 tracks/cm²). N_s is the number of counted spontaneous tracks, N is the number of successful grains analysed. ^{238}U is the average ^{238}U concentration, measured by LA-ICP-MS (in µg/g). Age (t) is given in Ma. For length data, l_m is the average confined track length, n is the number of confined tracks identified and measured and σc is the standard deviation of confined track lengths.

Sample	ρ_s	N_s	N	^{238}U	1σ	t (Ma)	l_m	n	σc
111	**17.983**	**428**	**12**	**29.602**	**0.504**	**152±14**	-	-	-
111A	6.914	56	3	4.066	0.103	258±38			
111B	23.694	372	9	38.114	0.637	133±7			
116	**55.459**	**1270**	**16**	**26.876**	**0.357**	**410±46**	-	-	-
116A	69.672	425	4	18.382	0.250	747±44			
116B	53.621	622	8	26.387	0.394	416±26			
116C	42.885	223	4	36.347	0.389	239±25			
126	**32.345**	**469**	**9**	**9.086**	**0.224**	**696±71**	-	-	-
126A	38.361	234	4	7.806	0.216	922±66			
126B	27.976	235	5	10.109	0.230	520±38			
127	**19.315**	**479**	**16**	**11.183**	**0.231**	**421±23**	-	-	-
952	**15.512**	**1531**	**20**	**6.067**	**0.139**	**442±23**	**11.66**	**47**	**2.38**
952A	15.450	893	11	4.863	0.090	521±20			
952B	15.279	576	9	6.953	0.178	358±17			
965	**47.912**	**2065**	**17**	**34.745**	**0.303**	**274±21**	**13.20**	**38**	**1.25**
965A	53.576	1618	11	32.966	0.248	330±8			
965B	34.651	447	6	38.008	0.406	193±9			
967	**18.184**	**1642**	**25**	**9.134**	**0.159**	**414±22**	**12.28**	**38**	**1.47**
967A	16.965	967	15	6.516	0.119	487±18			
967B	18.676	508	8	10.974	0.160	348±20			
967C	27.377	167	2	21.399	0.451	221±18			
972	**22.164**	**676**	**16**	**13.947**	**0.374**	**325±39**	**11.33**	**25**	**1.97**
972A	19.343	265	7	7.932	0.279	532±44			
972B	24.464	411	9	18.625	0.449	278±16			

Apatite and Zircon (U-Th-Sm)/He results

Apatite (U-Th-Sm)/He (AHe) and Zircon (U-Th-Sm)/He (ZHe) thermochronology was carried out on several samples in this study. Results from AHe and ZHe dating are summarised in Table 6, and Figures 5 & 6.

AHe ages were obtained for samples 952 and 972. Sample 952 yields a single AHe peak with a mean Devonian (396.9±24.6 Ma) age. This was based on the average age of five

single grain aliquots ranging from 345-435 Ma. This early Devonian AHe age corresponds very well with the youngest AFT peak of this sample (358±17 Ma), indicating that fast cooling occurred at that time. For sample 972 two AHe age peaks were distinguished, a Neoproterozoic (660.8±40.7 Ma) age and a late Triassic (217.1±14.0 Ma) age. These were both based on two single grain aliquot ages. The Neoproterozoic AHe age peak is older than the oldest AFT age peak which is likely the result of excess helium in the apatite crystals and is not discussed further. The late Triassic AHe age mimics its youngest AFT age-peak (278±16 Ma) which is indicative for fast cooling at that time.

ZHe ages were obtained for samples 972 and 111. Two ZHe age peaks are identified for sample 972, a Mesoproterozoic (1283.2±103.7 Ma) age and a Neoproterozoic (858.5±75.1 Ma) age. These were both based on two single grain aliquot ages. Given that these ZHe ages are much older than all AFT and AHe ages for the same sample, they likely reflect very slow cooling of the basement to upper crustal levels (slow passage through the ZHe closure temperature of ~200-180 ºC) during the Meso- to Neoproterozoic. Sample 111 yields three ZHe peaks, a late Ordovician (448.5±32.7 Ma) age, a late Triassic (214.8±14.2 Ma) age and an early Cretaceous (106.6±7.6) age. Both the Upper Ordovician and Upper Triassic age are only based on one single grain aliquot suggesting that they indicate partial resetting of an older event. The late Permian AFT age peak for this sample corresponds with the late Triassic ZHe age. Because of this, the age may be considered reliable even though it is based on one single grained aliquot only. The Lower Cretaceous age is based on two single grain aliquots and thus better reproducible and reliable.

Table 6: Apatite (U-Th-Sm)/He and Zircon (U-Th-Sm)/He dating results. Aqt = Aliquot number. Concentrations for Th, U, Sm are in ppm. Concentrations for ^{4}He are in ncc/µg. Ft is the α-ejection correction factor (Farley 2002). AHe and ZHe ages (t) are given in Ma. Age peaks within each sample are given including the aliquot numbers (on which the ages are based on).

Apatite (AHe)

Sample	Aqt	Th	± (%)	U	± (%)	Sm	± (%)	^{4}He	± (%)	Ft	t (Ma)	±	Peaks	Av. Age	±
972	1	55.76	4.13	14.53	4.34	56.28	0.20	0.20	3.12	0.56	212.0	14.0			
	2	211.57	4.08	33.70	4.43	105.56	0.93	0.66	2.45	0.56	222.1	14.0			
	3	102.75	4.11	37.32	4.33	80.19	0.62	1.29	1.55	0.52	784.8	47.5			
	4	129.12	4.10	29.17	4.43	64.65	0.72	0.67	2.40	0.49	536.8	33.8			
													One (2,3)	217.1	14.0
													Two (4,5)	660.8	40.7
952	1	353.37	4.07	105.19	4.375	48.69	0.55	16.13	2.50	0.73	434.6	27.6			
	2	243.86	4.08	29.97	4.367	72.76	0.75	4.15	1.74	0.68	399.6	24.4			
	3	234.24	4.08	24.07	4.310	69.98	0.59	3.34	1.91	0.67	392.8	24.3			
	4	255.86	4.08	28.67	4.348	109.12	0.51	2.74	1.79	0.64	411.9	25.3			
	5	143.52	4.08	23.34	4.340	55.84	0.69	1.07	1.98	0.60	345.3	21.2			
													One (1,2,3,4,5)	396.9	24.6

Table 6: Continued.

Zircon (ZHe)

Sample	Aqt	Th	± (%)	U	± (%)	Sm	± (%)	^{4}He	± (%)	Ft	t (Ma)	±	Peaks	Av. Age	±
111	1	11.06	2.00	51.5	1979.9	122.42	418.3	2.52	5.7	0.77	105.8	6.1			
	2	3.35	2.00	43.6	1907.9	35.18	710.8	2.50	8.0	0.67	107.3	9.2			
	3	5.27	2.00	29.8	1364.8	121.37	376.2	2.53	6.5	0.76	214.8	14.2			
	4	2.91	2.00	23.1	1056.5	139.63	323.8	2.52	7.0	0.73	448.5	32.7			
													One (1,2)	106.6	7.6
													Two (3)	214.8	14.2
													Three (4)	448.5	32.7
972	1	0.64	2.01	2.9	130.0	104.92	51.8	2.54	8.4	0.76	1317.5	111.9			
	2	0.67	2.01	13.3	509.6	57.70	189.3	2.51	8.1	0.63	891.1	76.9			
	3	0.69	2.01	8.0	368.7	60.89	145.8	2.53	8.4	0.69	825.8	73.3			
	4	0.83	2.01	3.6	165.1	121.40	54.8	2.51	7.4	0.74	1248.9	95.6			
													One (1,4)	1283.2	103.7
													Two (2,3)	858.5	75.1

HeFTy time-temperature models

Time-temperature models for samples 965, 967 and 972 are presented in Figure 7. Sample 965 is constrained by AFT age and length data only and exhibits a simple cooling history with protracted cooling throughout the Neoproterozoic and Palaeozoic. A pronounced cooling episode is shown to occur during the Triassic bringing the sample to near surface conditions. This correlates with the youngest AFT age peak for this sample.

Sample 967 is also constrained by AFT age and length data only. It exhibits a fairly simple cooling history showing that moderate to fast cooling occurred from the late Neoproterozoic to the Cambrian to upper crustal temperatures (~60-100 ºC). It remained within this temperature range until the Triassic where rapid cooling occurred to near surface conditions, similar to the cooling episode seen in sample 965.

Sample 972 exhibits a more complex thermal history and is based on AHe data as well as AFT. It shows that this sample was most likely brought to temperatures between approximately 50-80 ºC somewhere between the late Neoproterozoic to the Ordovician. This was followed by a slight increase in temperature before fairly rapid cooling occurred during the Permian. The constraint that is responsible for this Permian cooling event was required to run the HeFTy model. Subsequently, shallow reheating occurred during the Triassic followed by a new event of cooling during the early Jurassic. From the late Jurassic onwards sample 972 remained at near surface temperatures below 50 ºC until the present day.

It was not possible to calculate a HeFTy model for sample 952 due to discrepancy between the track length histogram and the obtained AHe data for this sample. The length histogram appears bimodal and asks for multiple cooling and reheating events, while the AHe data mimics the AFT data of 358±17 Ma which suggest a simple cooling model. Due to the low amount of fission track length data, the latter model is favoured.

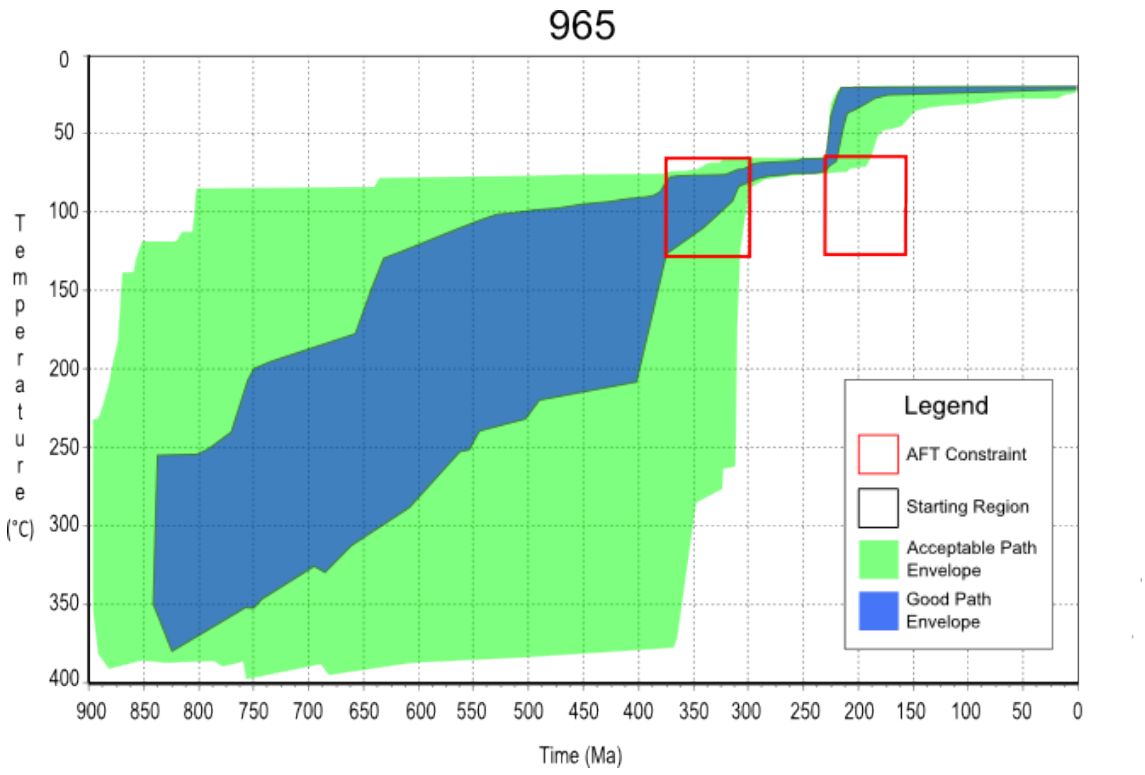

Figure 7: Time-Temperature models for samples 965, 967 and 972. These were constructed using the modelling software HeFTy (Ketcham 2005). Low-T thermochronological constraints for the models are shown as boxes with different colours representing the different low-T methods used in this study. The dashed constraint in the model for sample 972 was required to run the model and is not constrained by independent thermochronological data. Acceptable cooling path envelopes are shown in green, statistical good fit path envelopes are shown in blue. For sample 965 and 967 the default merit value for good paths of 0.5 and merit of value for acceptable paths of 0.05 was used. Models for these samples are based on AFT age and length data only and produce fairly simple cooling models. Sample 972 is based on a larger dataset including AHe data as well and consequently required a lower merit value for good fit paths of 0.2. Sample 972 exhibit a more complex thermal history. Those samples for which no length data could be obtained are not modelled. Sample 952 was not able to be modelled due to discrepancy between the track length histogram and the obtained AHe data for this sample.

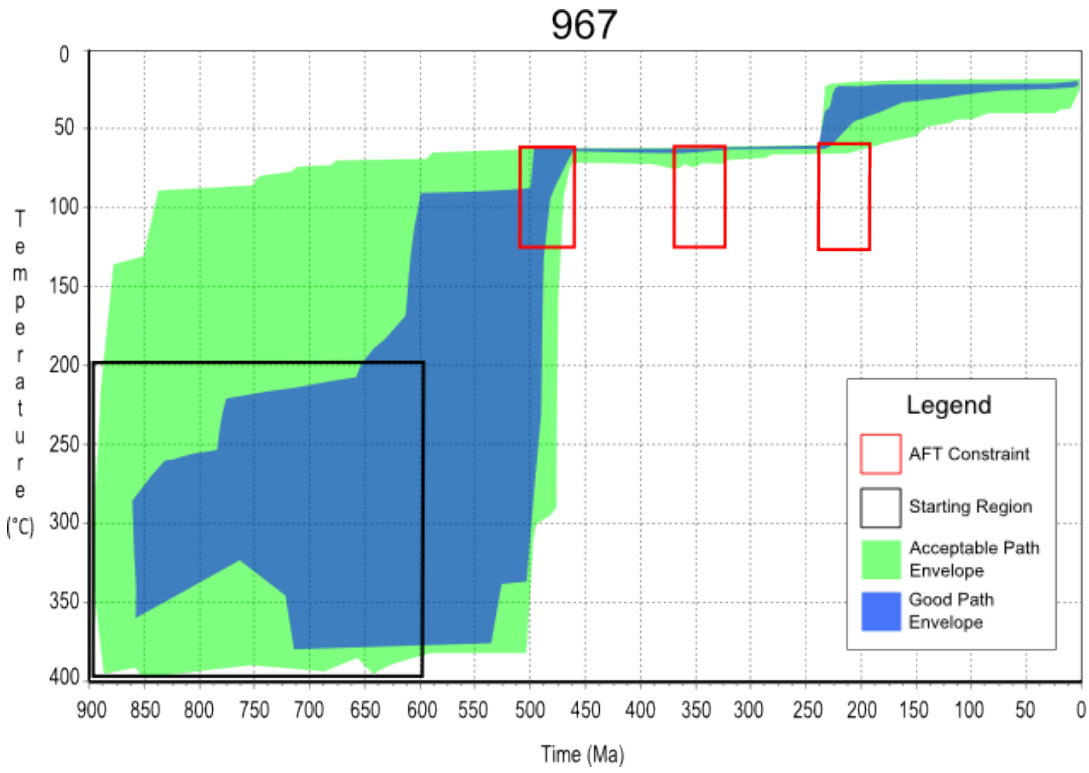

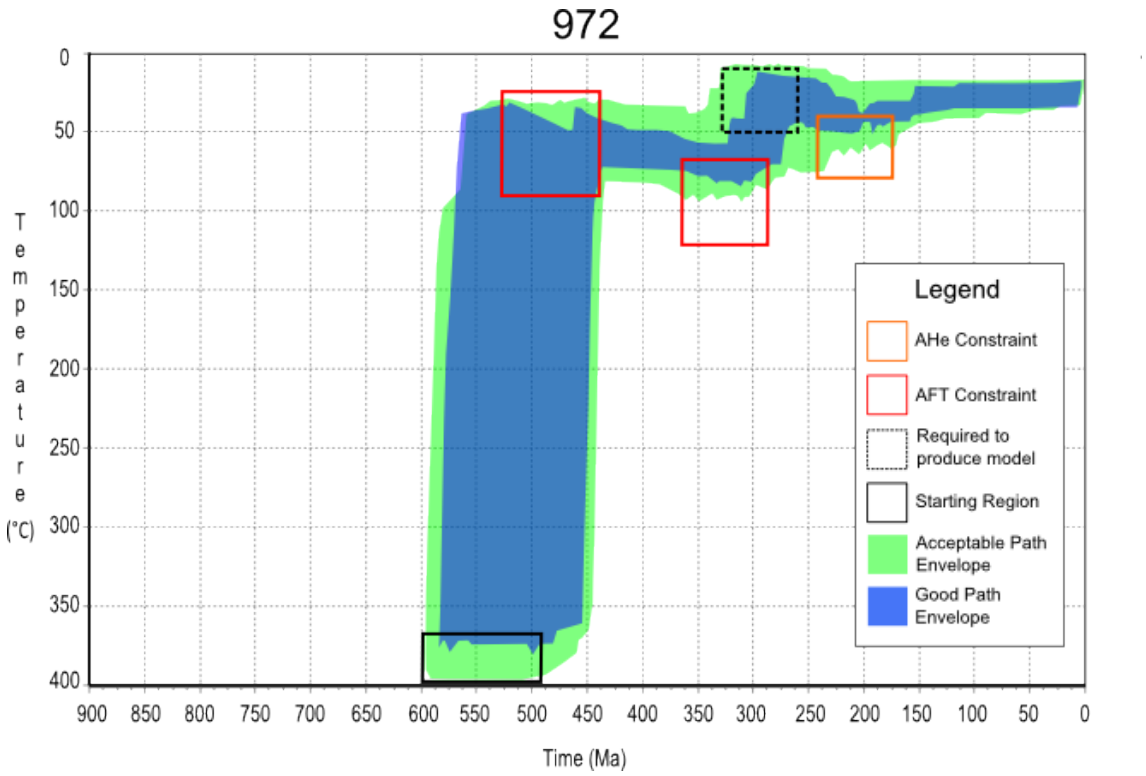

Figure 7: Continued.

DISCUSSION

Cumulative AFT data

The thermochronological data presented here indicate several low-temperature thermal events to have occurred in the central and northern Gawler Craton throughout the Neoproterozoic and Phanerozoic. Figure 8 shows a pooled radial plot of all data obtained for this thesis. Cooling ages range from the Neoproterozoic through to the Cretaceous.

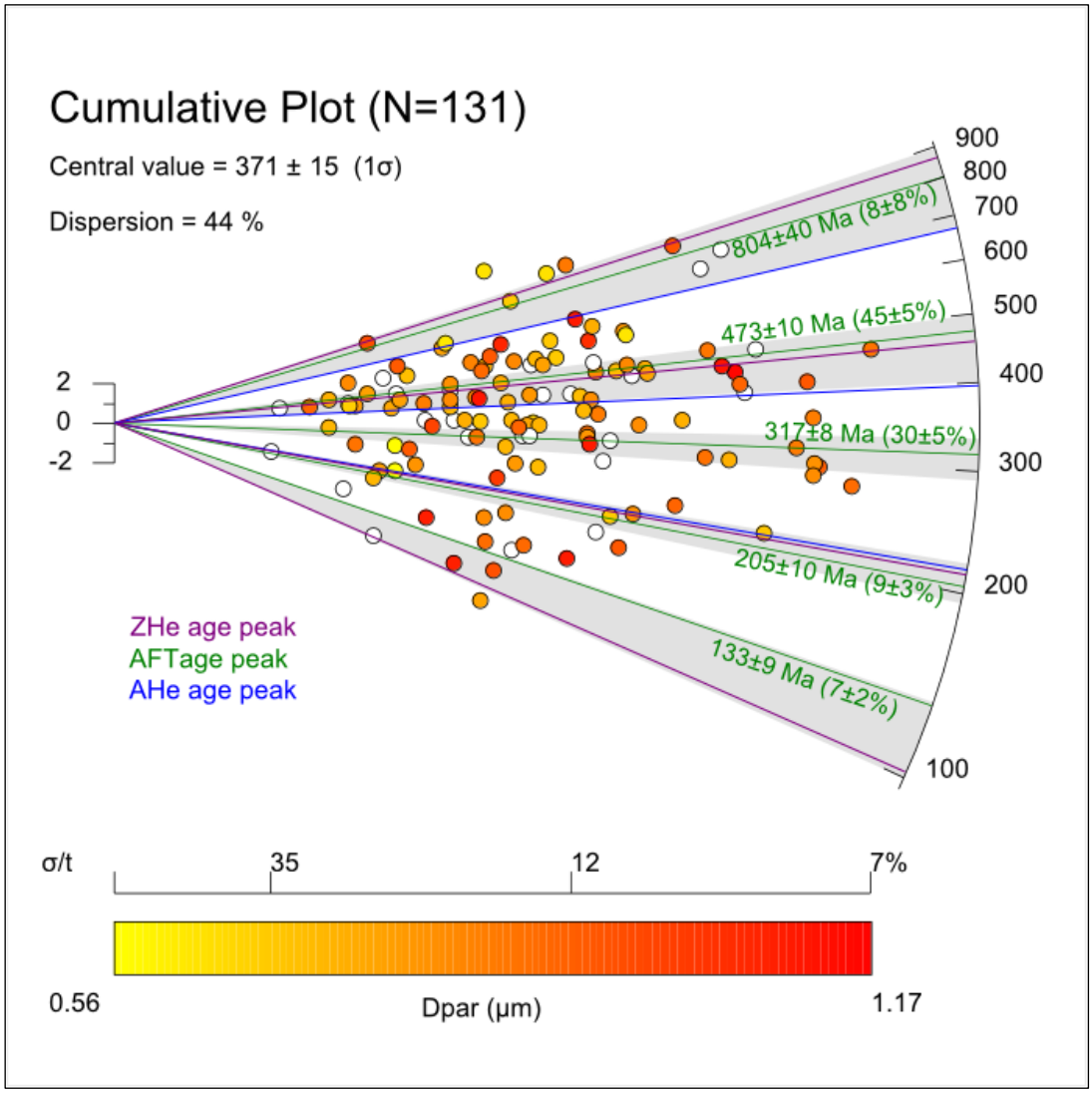

Figure 8: Cumulative radial plot of all AFT ages produced in this study demonstrating the AFT age peaks. Constructed using the software program RadialPlotter (Vermeesch 2009). For a description on radial plots see Figures 3 & 6. Five AFT age peaks are defined. ZHe and AHe age peaks are included as well. Grey zones highlight the cumulative age peaks of this study based on all low-T chronometers applied.

The Neoproterozoic (~800 Ma) AFT age peak is the oldest and least significant peak to be defined in this study. It is essentially constrained by single grain ages from samples 126, 116 and to a lesser extent 972 in the central and northeast of the study region. This peak corresponds well with the slightly older Mesoproterozoic (1283±104 Ma) and Neoproterozoic (858±78 Ma) ZHe age peaks produced for sample 972. No major tectonothermal events are recorded in the literature for the Gawler Craton in this time period. Because of this, and the fact this peak is poorly constrained, we do not make any major interpretations. We suggest these ages are probably a result of protracted cooling through the AFT PAZ during the Neoproterozoic, as a result of prolonged exhumation of the Gawler Craton at that time.

A well-defined Ordovician (~470 Ma) AFT age peak was obtained and observed in most samples for this study. Sample 111 in the far north contains no AFT age peaks for this period. However, it's late Ordovician (449±33 Ma) ZHe age peak does resemble the AFT age peak closely. This indicates that this sample remained at higher temperatures (between ~200 and 120 ºC) and presumably deeper crustal levels throughout this event, compared with samples to the south and illustrates that the extent of this cooling phase varies throughout the study region. The time-temperature models for sample 967 and 972 (Figure 7) show that this cooling event brought the sampled rocks relatively rapidly to the sub-surface at that time. A large number of Ordovician AFT ages have previously been reported for the central Gawler Craton as well (Figure 9; Gleadow et al. 2002, Kohn et al. 2002, Boone 2013). Rather than being clustered to the Ordovician, these previously obtained AFT ages span most of the Palaeozoic and are previously interpreted as the result of prolonged cooling and exhumation of the Gawler Craton at

that time. The late Cambrian-Ordovician AFT ages obtained for this thesis are more tightly clustered and mimicked by ZHe and AHe constraints as well and suggest the onset of a regional moderate to fast cooling event at that time. We interpret this late Cambrian – Ordovician cooling event to be largely a result of the Delamerian Orogeny (514-490 Ma) (Foden. et al. 2006) which may have been enhanced during the onset of the Alice Springs Orogeny at ~450 Ma (Raimondo et al. 2014). The sedimentary record contains no sedimentary formations that were deposited throughout or immediately after the Ordovician to support evidence for rapid exhumation at that time, which may indicate that these sediments have been reworked during subsequent events.

For most samples a Carboniferous (~320 Ma) AFT age peak was obtained. This is constrained in varying degrees by single grain ages from all samples in this study, except sample 126 and perhaps sample 111 that appears to be overprinted almost entirely by younger events. It is most pronounced in samples 965 and 967 (in the south of the study area) which were sampled in close vicinity to previously studied AFT samples where similar well-defined Carboniferous-AFT ages were obtained, centred at 327.4±1.6 Ma (centered at ~327 Ma; Gleadow et al. 2002, Kohn et al. 2002, Boone 2013; Fig. 9). The significance of this Carboniferous AFT age peak is disputable, especially since it is not supported by other thermochronological constraints. Boone (2013) argued that these ages represent slow cooling through the APAZ as the result of prolonged Palaeozoic exhumation of the Gawler Craton. This may explain why the HeFTy models for samples 965 and 967 show no clear cooling event during the Carboniferous as well (e.g. the time-temperature model for sample 965 shows steady cooling throughout the early Palaeozoic until the late Carboniferous). However, the

time-temperature model for sample 972 which is based on a larger dataset requires a more pronounced Carboniferous cooling event. This may indicate that the slow exhumation of the Gawler Craton was somewhat enhanced during the Carboniferous, potentially as a far-field response to the final stages of the Alice Springs Orogeny (Sandiford and Hand 1998, Raimondo et al. 2014). Carboniferous AFT ages have previously been obtained for the Officer Basin (Tingate and Duddy 2002) and within the Adelaide Fold Belt (Mitchell et al. 1998, Gibson and Stüwe 2000) as well which suggests that the Carboniferous pulse of the Alice Springs Orogeny may have affected southern and central Australia on a regional scale.

The next cumulative age peak in the AFT data is late Triassic (~205 Ma) in age. Given that not all samples exhibit late Triassic – early Jurassic AFT data, this age-peak likely represents a localised event. For sample 972 a late Triassic AHe age was obtained which corresponds well with the late-Triassic – early Jurassic AFT age peak, suggesting that localised fast cooling occurred at that time. Sample 111 yields a single ZHe age of 215±14 Ma which corresponds well with this AFT age peak as well. However, given that this sample was largely reset during a subsequent event, it is not clear whether this ZHe age represents a well-defined event or rather a mixing age between two other events. The time-temperature models for samples 965 and 967 both show fairly rapid exhumation during the Triassic from ~70 ºC to near surface temperatures. The time temperature model for samples 972 does not require a major cooling event at this time, but does allow for some cooling after a reheating occurred during the Triassic. Given the dominant tectonic regime for southern Australia at the time, we infer that the late Triassic and early Jurassic low-T thermochronological ages produced here record a far-

field effect of the initial development of the southern ocean rift during the breakup of Gondwana (Veevers et al. 1991, Drexel and Preiss 1995). We suggest that this process induced exhumation across the entire study region although the extent of this exhumation event varies largely between the different sampling locations. Triassic-Jurassic AFT ages have been found within the Adelaide Fold Belt, particularly on the Yorke Peninsula (Gibson and Stüwe 2000). Similar ages have also been found on the Eyre Peninsula, particularly along the eastern coastline (Figure 9; Boone 2013, Gleadow et al. 2002, Kohn et al. 2002).

The youngest cumulative AFT age peak in the data is Cretaceous (133±9 Ma) in age. This is almost entirely constrained by sample 111 in the far north of the study region. Therefore, the individual Cretaceous (108±23 Ma) AFT age peak for this individual sample is a better indication of the timing of Cretaceous cooling. No time-temperature models were able to be produced for this sample due to a lack of confined track length data. Nevertheless, the Cretaceous (107±7 Ma) ZHe age obtained for this sample illustrates the significance of this AFT age peak and indicates that this sample underwent very rapid cooling during the middle Cretaceous. No other samples in the study region have produced ages this young. Approximately 40km to the southeast, sample 126 yields a Cambrian (512±51 Ma) minimum AFT age. For sample 116, which was taken ~50km to the south of sample 111, a Triassic (223±28 Ma) minimum AFT age was obtained. These ages illustrate that the Cretaceous thermal event that reset the thermochronometric clocks for sample 111 was fairly localised. The localised nature may reflect deep exhumation e.g. by river incision. Figure 9 shows the approximate location of the Garford and Kingoonya palaeochannels. Sample 111 plots very close to

the mapped location of the Garford Palaeochannel, suggesting that the Cretaceous resetting is a result of river incision at that time. This exhumation correlates with the widespread late Cretaceous exhumation event throughout southern Australia proposed in (Macdonald et al. 2013). This was based on a large population of Cretaceous and even Cenozoic AFT ages that were produced in parts of south central Australia including the southern Musgrave Block, western Eromanga Basin, Officer Basin, Flinders Ranges, Yorke Peninsula, southern Adelaide Fold Belt and Kangaroo Island (Mitchell et al. 1998, Gibson and Stüwe 2000, Tingate and Duddy 2002, Tingate et al. 2007). Alternatively, it could be argued that this sample did not experience Cretaceous exhumation, and instead underwent resetting by hydrothermal fluids. This would help explain why these Cretaceous ages are not seen in nearby samples as well. A similar interpretation was made for samples in the central Gawler Craton where a Cenozoic (41.3±1.6 Ma) AFT age peak was identified (Gleadow et al. 2002, Kohn et al. 2002, Boone 2013). These authors argued that due to the lack of structural and stratigraphic constrains along with the nearness to the Eromanga Basin, it was most likely that hydrothermal fluids were the source for Cretaceous-Palaeogene thermal overprinting. Two samples that contribute to this Cenozoic age peak are located within the Kingoonya palaeochannel (Figure 9) and yield Cretaceous (119±20 Ma) and Paleogene (35±4 Ma) AFT ages. As a result, river incision should be considered as a possible explanation for the late Mesozoic-Cenozoic AFT ages seen in these previous studies as well. Whether the Cretaceous cooling ages produced in this study are the result of exhumation related with river incision or hydrothermal alteration is not clear and more data is required to confirm one of these interpretations.

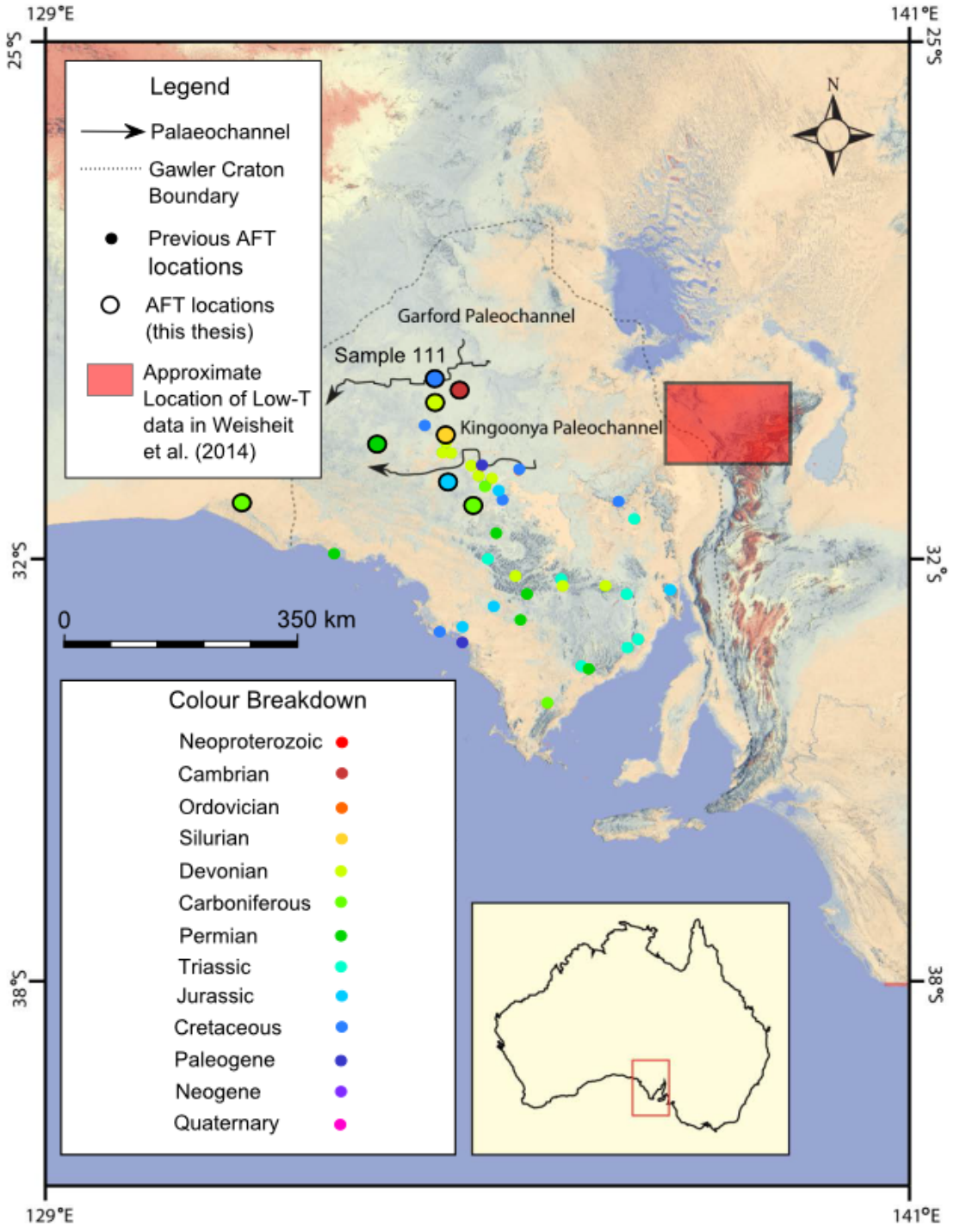

Figure 9: Digital elevation model with indication of previous AFT data obtained for the Gawler Craton (Gleadow et al. 2002, Kohn et al. 2002, Boone 2013). The locations of samples for this study are indicated by larger circles and colour code following their youngest AFT age peak. Modified from Boone (2013). The approximate location of the Garford and Kingoonya Palaeochannels are included. This demonstrates that sample 111 lies within the Garford Palaeochannel and provides a possible explanation for the anomalously young low-T ages yielded for this sample.

Cumulative time-temperature history

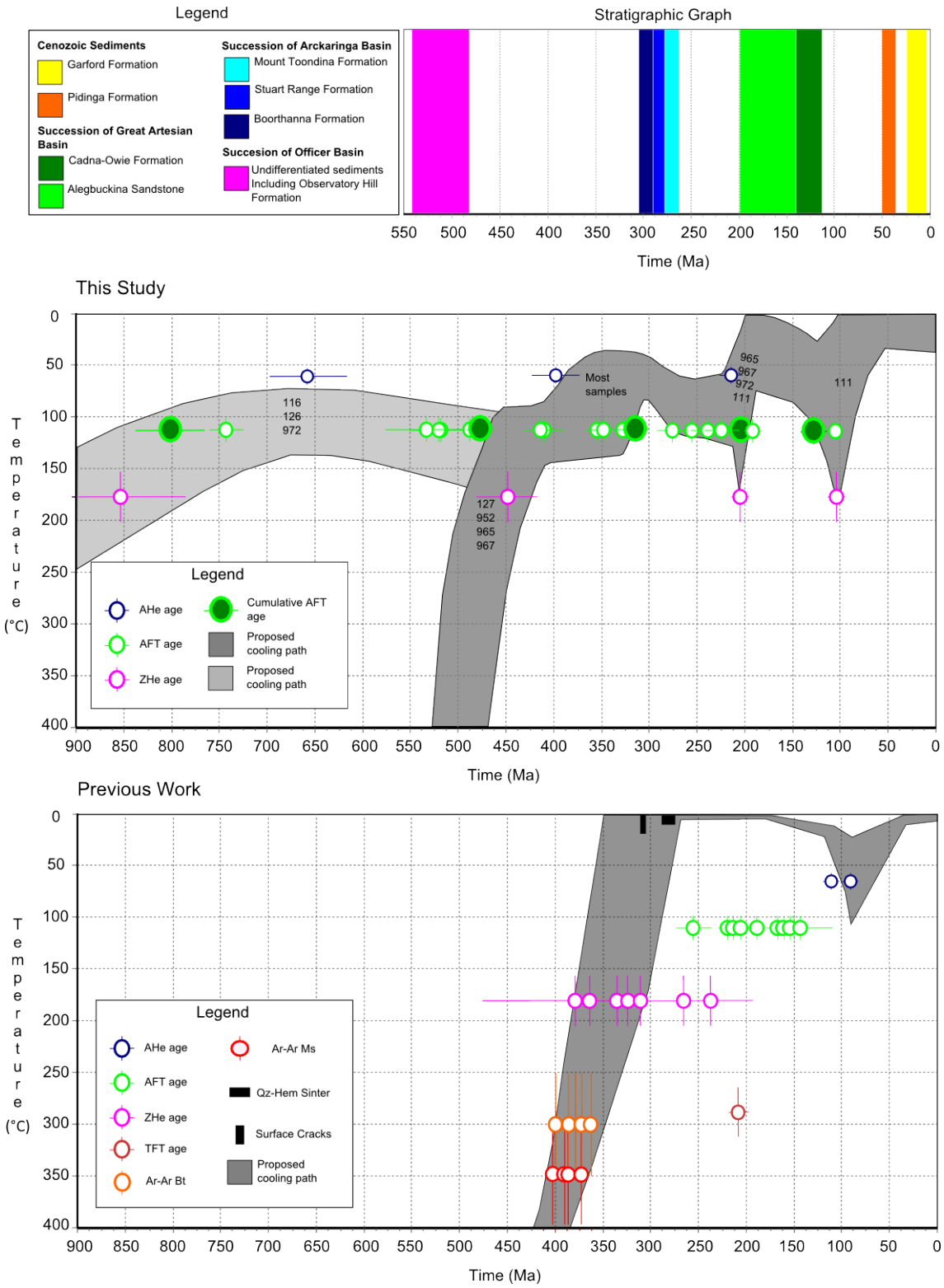

Figure 10: Time-temperature plots showing all low-T thermochronometric data and proposed thermal history models for this study compared to the model presented by Weisheit et al. (2014). Later work includes low-T data from several studies in the northern Flinders Ranges area, east of the study region for this thesis (indicated on Figure 9). A stratigraphic graph of the major

sedimentary formations within the study area is included. Formations that were deposited in exclusively marine environments including the Bulldog Shale were omitted as they are not a reliable indicator for exhumation. Within each plot, different low-T techniques are presented in different colours. For this study, the proposed cooling path is a best estimate for the entire study region. The cooling path is annotated to indicate which samples experienced the various thermal events. The lighter grey cooling path illustrates constrains the pre-Phanerozoic cooling that was observed for some samples.

Figure 10 shows the best estimate for the low-temperature thermal history of the Gawler Craton, based on all data for this study compared to the proposed thermal history model for the northern Flinders Ranges (Weisheit et al. 2014). Samples 116, 126 and 972 record evidence for the pre-Phanerozoic thermal history of the study region, which is outlined in light grey on the figure. All remaining samples are shown to be exhumed from greater temperatures during the early Palaeozoic, either as a result of the Delamerian Orogeny or the onset of the Alice Springs Orogeny. Subsequent Carboniferous cooling during the final stages of the Alice Springs Orogeny likely exhumed the sampled rocks to shallow-crustal levels. Following this exhumation event, the sedimentary record is dominated by three sedimentary successions of the Arckaringa Basin, which were deposited in a variety of depositional environments (see Table 3). These sediments likely represent the preserved erosion products of the Carboniferous exhumation phase. Subsequent minor heating of all samples is interpreted in response to sedimentary burial. Samples 116, 126, 127 and 952 yield minimal Mesozoic AFT ages and are therefore not thought to experience any subsequent cooling events. Samples 111, 965, 967 and 972 record Late Triassic-Early Jurassic cooling and define the Mesozoic thermal history of Figure 10. This event is followed by sedimentation associated with the Eromanga Basin (part of the Great Artesian Basin) within the study area, which induced minor reheating by shallow burial. The youngest cooling event during the Cretaceous only applies to sample 111. It demonstrates the rapid Cretaceous

exhumation or hydrothermal reset that is interpreted for this sample. Cenozoic cooling ages were not obtained in this study, suggesting thermal quiescence throughout the Cenozoic in the Gawler Craton.

Figure 10 also includes a time-temperature model based on previous low-T thermochronometric studies from the northern Flinders Ranges region (Weisheit et al. 2014). No low-T data from the northern Flinders Ranges is indicative of prolonged cooling in the Neoproterozoic. However, the proposed exhumation paths shows fast cooling from lower crustal levels occurring throughout the duration of the Alice Springs Orogeny. This coincides with the proposed exhumation path for most samples in this study. This demonstrates how widespread the effects of the Alice Springs Orogeny were likely to be. Unlike the data produced in this thesis, surface constraints require that exhumation in the northern Flinders Ranges region during this cooling event brought samples to surface temperatures. Mesozoic AFT ages plot well outside of the proposed exhumation path for the northern Flinders Ranges and are thought to be a result of resetting related to a near-surface hydrothermal event (Weisheit et al. 2014). The same interpretation is made for the Cretaceous AHe ages which have been used to propose reheating and subsequent cooling during this time. This final cooling event is synchronous with the rapid Cretaceous cooling found in sample 111 from this study, but from much lower temperatures.

CONCLUSIONS

The low-T thermochronological data produced in this thesis imply a complex Phanerozoic low-T thermal history of the central and northern Gawler Craton. Five main thermal events were identified within the study region. Neoproterozoic AFT ages

throughout the region are interpreted as protracted cooling as a result of prolonged exhumation of the Gawler Craton. Slightly younger low-T ages and time-temperature models indicate this prolonged exhumation was punctuated by increased Ordovician exhumation within the central and northern Gawler Craton. This was most likely a result of the Delamerian Orogeny and/or the early phases of the Alice Springs Orogeny. Following this, the latest stages of the Alice Springs Orogeny are thought to have induced minor regional exhumation throughout the study area as well during the Carboniferous (350-300 Ma). From the late Triassic, southern Australia was dominated by a new tectonic regime. Rifting on Australia's southern margin began during the breakup of the Gondwana supercontinent. We suggest that the late Triassic and early Jurassic cooling ages produced in this thesis reflect exhumation of the study area in response to rifting at the newly formed continental margin. One sample from the far north of the study area exhibits thermal reset during the middle Cretaceous. This thermal event induced heat in excess of ~200 ºC, resetting the zircon U-Th-Sm/He clock. Given that this event was not observed in nearby samples to the south and southeast, this thermal event is likely to be quite localised and may reflect hydrothermal alteration or localised exhumation related with e.g. incision by an extensive river system.

ACKNOWLEDGMENTS

Dr. Stijn Glorie (The University of Adelaide)
Prof. Alan Collins (The University of Adelaide)
Dr. Katherine Howard (The University of Adelaide)
Dr. Rosalind King (The University of Adelaide)
Anthony Reid (DMITRE)
Claire Wade (DMITRE)
Aoife McFadden (Adelaide Microscopy)
Ben Wade (Adelaide Microscopy)

REFERENCES

(PIRSA) D. O. P. I. A. R. S. A. 2009 Tarcoola SH5310 map sheet, Coober Pedy SH330 map sheet.

ALEXANDER E. M. & HIBBURT J. 1996 Petroleum Geology of South Australia. In (PIRSA) D. O. P. I. A. R. S. A. ed. pp. 1999. Adelaide, South Australia.

BOONE S. C. 2013 Apatite Fission Track Anomaly within the Archean-Proterozoic Gawler Craton: The Thermal Record of a Paleoaquifer System? School of Earth Sciences. pp. 200. Melbourne: University of Melbourne.

DE GRAVE J., GLORIE S., RYABININ A., ZHIMULEV F., BUSLOV M. M., IZMER A., ELBURG M., VANHAECKE F. & VAN DEN HAUTE P. 2012, Late Palaeozoic and Meso-Cenozoic tectonic evolution of the southern Kyrgyz Tien Shan: Constraints from multi-method thermochronology in the Trans-Alai, Turkestan-Alai segment and the southeastern Ferghana Basin, *Journal of Asian Earth Sciences* **44**, 149-168.

DREXEL J. F. & PREISS W. V. 1995 The Geology of South Australia. Geological Survey, South Australia.

EHLERS T. A. & FARLEY K. A. 2003, Apatite (U–Th)/He thermochronometry: methods and applications to problems in tectonic and surface processes, *Earth and Planetary Science Letters* **206**, 1-14.

ETHERIDGE M., MCQUEEN H. & LAMBECK K. 1991, The role of intraplate stress in tertiary (and mesozoic) deformation of the Australian continent and its margins: A key factor in petroleum trap formation, *Exploration Geophysics* **22**, 123-128.

FANNING C. M., FLINT R. B., PARKER A. J., LUDWIG K. R. & BLISSETT A. H. 1988, Refined Proterozoic evolution of the Gawler Craton, South Australia, through U-Pb zircon geochronology, *Precambrian Research* **40–41**, 363-386.

FARLEY K. A. 2002, (U-Th)/He Dating: Techniques, Calibrations, and Applications, *Reviews in Mineralogy and Geochemistry* **47**, 819-844.

FODEN. J., ELBURG M. A., DOUGHERTY-PAGE. J. & BURTT A. 2006, The Timing and Duration of the Delamerian Orogeny: Correlation with the Ross Orogen and Implications for Gondwana Assembly, *Journal of Geology* **114**, 189-210.

FOSTER D. A., MURPHY J. M. & GLEADOW A. J. W. 1994, Middle tertiary hydrothermal activity and uplift of the northern flinders ranges, South Australia: Insights from apatite fission-track thermochronology, *Australian Journal of Earth Sciences* **41**, 11-17.

GALE S. J. 1992, Long-term landscape evolution in Australia, *Earth Surface Processes and Landforms* **17**, 323-343.

GEOSCIENCE-AUSTRALIA 2014 Australian Stratigraphic Units Database.

GIBSON H. J. & STÜWE K. 2000, Multiphase cooling and exhumation of the southern Adelaide Fold Belt: constraints from apatite fission track data, *Basin Research* **12**, 31-45.

GLEADOW A. J. W., KOHN B. P., BROWN R. W., O'SULLIVAN P. B. & RAZA A. 2002, Fission track thermotectonic imaging of the Australian continent, *Tectonophysics* **349**, 5-21.

GLORIE S., DE GRAVE J., VAN DEN HAUTE P. & ELBURG M. 2010 Evaluating the effect of anisotropy on fossil fission track length distributions in apatite. THERMO2010, proceedings from the 12th International Conference on thermochronology. Glasgow, UK.

GREEN P. F., DUDDY I. R., GLEADOW A. J. W., TINGATE P. R. & LASLETT G. M. 1986, Thermal annealing of fission tracks in apatite: 1. A qualitative description, *Chemical Geology: Isotope Geoscience section* **59**, 237-253.

GURNIS M. R. D. L. 1998, Cretaceous vertical motion of Australia and the Australian-Antarctic discordance, *Science* **279**, 1499-1504.

HAND M., REID A. & JAGODZINSKI L. 2007, Tectonic Framework and Evolution of the Gawler Craton, Southern Australia, *Economic Geology* **102**, 1377-1395.

HASEBE N., BARBARAND J., JARVIS K., CARTER A. & HURFORD A. J. 2004, Apatite fission-track chronometry using laser ablation ICP-MS, *Chemical Geology* **207**, 135-145.

HOWARD K. E., HAND M., BAROVICH K. M., PAYNE J. L., CUTTS K. A. & BELOUSOVA E. A. 2011, U–Pb zircon, zircon Hf and whole-rock Sm–Nd isotopic constraints on the evolution of Paleoproterozoic rocks in the northern Gawler Craton, *Australian Journal of Earth Sciences* **58**, 615-638.

KETCHAM R. A. 2005 HeFTy Version 1.8.2 ed.: Apatite to Zircon, Incorporated.

KOHN B. P., GLEADOW A. J. W., BROWN R. W., GALLAGHER K., O'SULLIVAN P. B. & FOSTER D. A. 2002, Shaping the Australian crust over the last 300 million years: insights from fission track thermotectonic imaging and denudation studies of key terranes, *Australian Journal of Earth Sciences* **49**, 697-717.

LI G.-M., CAO M.-J., QIN K.-Z., EVANS N. J., MCINNES B. I. A. & LIU Y.-S. 2014, Thermal-tectonic history of the Baogutu porphyry Cu deposit, West Junggar as constrained from zircon U–Pb, biotite Ar/Ar and zircon/apatite (U–Th)/He dating, *Journal of Asian Earth Sciences* **79, Part B**, 741-758.

MACDONALD J. D., HOLFORD S. P., GREEN P. F., DUDDY I. R., KING R. C. & BACKE G. 2013, Detrital zircon data reveal the origin of Australia's largest delta system, *Journal of the Geological Society, London* **170**, 3-6.

MCDOWELL F. W., MCINTOSH W. C. & FARLEY K. A. 2005, A precise 40Ar–39Ar reference age for the Durango apatite (U–Th)/He and fission-track dating standard, *Chemical Geology* **214**, 249-263.

MITCHELL M. M., KOHN B. P. & FOSTER D. A. 1998 Post-Orogenic Cooling History of Eastern South Australia from Apatite FT Thermochronology. In HAUTE P. & CORTE F. eds. Advances in Fission-Track Geochronology. pp. 207-224. Springer Netherlands.

MITCHELL M. M., KOHN B. P., O'SULLIVAN P. B., HARTLEY M. J. & FOSTER D. A. 2002, Low-temperature thermochronology of the Mt Painter Province, South Australia, *Australian Journal of Earth Sciences* **49**, p.551.

O'SULLIVAN P. B. & PARRISH R. R. 1995, The importance of apatite composition and single-grain ages when interpreting fission track data from plutonic rocks: a case study from the Coast Ranges, British Columbia, *Earth and Planetary Science Letters* **132**, 213-224.

PAYNE J. L., BAROVICH K. M. & HAND M. 2006, Provenance of metasedimentary rocks in the northern Gawler Craton, Australia: Implications for Palaeoproterozoic reconstructions, *Precambrian Research* **148**, 275-291.

RAIMONDO T., HAND M. & COLLINS W. J. 2014, Compressional intracontinental orogens: Ancient and modern perspectives, *Earth-Science Reviews* **130**, 128-153.

SANDIFORD M. & HAND M. 1998, Controls on the locus of intraplate deformation in central Australia, *Earth and Planetary Science Letters* **162**, 97-110.

SANDIFORD M. 2007, The tilting continent: A new constraint on the dynamic topographic field from Australia, *Earth and Planetary Science Letters* **261**, 152-163.

SWAIN G. M., HAND M., TEASDALE J., RUTHERFORD L. & CLARK C. 2005, Age constraints on terrane-scale shear zones in the Gawler Craton, southern Australia, *Precambrian Research* **139**, 164-180.

TAGAMI T. & O'SULLIVAN P. B. 2005, Fundamentals of Fission-Track Thermochronology, *Reviews in Mineralogy and Geochemistry* **58**, 19-47.

TINGATE P. R. & DUDDY I. R. 2002, The thermal history of the eastern Officer Basin (South Australia): evidence from apatite fission track analysis and organic maturity data, *Tectonophysics* **349**, 251-275.

TINGATE P. R., GREEN P. F., LEMON N. M. & MCKIRDY D. M. 2007 Insights into the tectonic development and hydrocarbon potential of the Flinders Ranges, South Australia, based on AFTA® and organic maturity data from the Blinman-2 borehole. Conference Proceedings of the Central Australian Basins Symposium. pp. 71-81.

VEEVERS J., MCA C. & ROOTS S. 1991, Review of seafloor spreading around Australia. I. Synthesis of the patterns of spreading, *Australian Journal of Earth Sciences* **38**, 373-389.

VERMEESCH P. 2009 Radial Plotter: A Java application for fission track, luminescence and other radial plots. Radiation Measurements 44, 409-410

WAGNER G. A. & VAN DEN HAUTE P. 1992 Fission Track-Dating. Kluwer Academic Publishers, Dordrecht, the Netherlands.

WEBB A. W., THOMSON B. P., BLISSETT A. H., DALY S. J., FLINT R. B. & PARKER A. J. 1986, Geochronology of the Gawler Craton, South Australia, *Australian Journal of Earth Sciences* **33**, 119-143.

WEISHEIT A., BONS P. D., DANISÍK M. & ELBURG M. A. 2014, Crustal-scale folding: Palaeozoic deformation of the Mt Painter Inlier, South Australia, *Geological Society, London, Special Publications* **394**, 53-77.

WOLF R. A., FARLEY K. A. & KASS D. M. 1998, Modeling of the temperature sensitivity of the apatite (U–Th)/He thermochronometer, *Chemical Geology* **148**, 105-114.

WOLFE M. R. & STOCKLI D. F. 2010, Zircon (U–Th)/He thermochronometry in the KTB drill hole, Germany, and its implications for bulk He diffusion kinetics in zircon, *Earth and Planetary Science Letters* **295**, 69-82.

YU S., CHEN W., EVANS N. J., MCINNES B. I. A., YIN J., SUN J., LI J. & ZHANG B. Cenozoic uplift, exhumation and deformation in the north Kuqa Depression, China as constrained by (U–Th)/He thermochronometry, *Tectonophysics*.

APPENDIX A: EXTENDED METHODS

Apatite Fission Track Thermochronology

Sample Acquisition: Apatite Fission Track analysis was carried out on 13 Samples in the northern Gawler Craton and surrounds. These samples were collected in the field by Anthony Reid (DMITRE). Nine of these samples (2016111, 2016114, 2016116, 2016120, 2016122, 2016124, 2016126, 2016127 and Cairn Hill) were collected as whole rock samples while samples 2017952, 2017963, 2017964, 2016965, 2017967, 2017972 were received as mineral separates.

Sample Preparation: The whole rock samples required crushing before mineral separation that could later be used to obtain suitable apatite grains for analysis. Crushing and mineral separation was conducted in the laboratories within The University of Adelaide's Mawson Building. Samples were crushed and separated using conventional magnetic and heavy liquid techniques as explained below.

Lab training was conducted by Dr Katherine Howard (The University of Adelaide) during lab training sessions. All procedures outlined in these sessions were followed. Cleaning procedures outlined in lab training and on posters within each of the three laboratories were adhered too before and after work was done on each sample. This was particularly important in preventing contamination of any samples. Appropriate safety gear was worn including safety glasses, ear muffs and lab coats.

All rocks samples were initially washed thoroughly using running water and a scrubbing brush to remove any detrital apatite from the surface of samples. The Rock Saw was used to break large samples into approximately 10x10x10cm blocks. This was achieved by turning the machine on (green start-up button), ensuring the water feeding into the grinding disc was on and applying an even pressure as the sample was pushed through the saw. Wooden blocks were used to hold smaller rock samples in place to help prevent injuries to the hand or other parts of the body. The Rock Saw was turned off using the red stop button. The saw was cleaned by rinsing with water using the hose found on top of the machine.

Crushing: Crushing of samples was undertaken in the Crushing Room. Crushed samples were transferred from the Large Jaw Crusher, the Pulverisette Disc Mill and Sieve Shaker using A3 sheets of butcher's paper. Initial crushing of samples was performed using the Large Jaw Crusher. This crusher was cleaned before and after use by following five steps; blowing high pressured air using the air gun, ensuring all rock chips were removed using a metal prod, scrubbing with a brush, wiping with paper towel and ethanol before using the air gun for a second time. Samples were crushed by turning the machine on (green start-up button) and opening the hood before dropping samples into the machine while ensuring the hood was shut immediately while crushing occurred. A representative portion of the rock samples was put into the crusher whilst saving a small portion of each sample for potential future geochemical analysis. Crushed samples were transferred to the disc mill where they were further crushed.

The Disc Mill was cleaned before and after use in three steps; blowing high pressured air using the air gun, wiping with paper towel and ethanol before using the air gun once again. The two discs within the Disc Mill were set approximately 2mm apart using the lever. To start the machine the green start-up button was used. Partially crushed sampled were fed into the machine with the help of a paintbrush. Once the sample had run through the Disc Mill the machine was turned off using the red stop button. The sample was collected from the tray at the bottom of the disc mill and transferred to the Sieve that sat within the Sieve Shaker. The Sieve Shaker and the items used in constructing the Sieve were cleaned following the same steps as the disc mill before and after their use. The Sieve was constructed for each sample by placing the blue base plate on the bench. The Sieve was then built upwards in the following order; lower plate, fine sieve mesh, upper plate, lower plate, coarse sieve mesh, upper plate, sieve lid. The Sieve was then placed in the Sieve Shaker. The Sieve Shaker was turned on using the on switch at the front of the machine. The machine was run until a significant portion of the sample had penetrated the coarse mesh and fine mesh. The various particle sizes within the Sieve were placed into separate sealable bags and labelled accordingly. The grains within the 79-425µm size range were used in mineral separation.

Mineral Separation: Mineral separation took place in the Mineral Separation Room. Cleaning procedures listed on a poster within the room were followed. Separation required three main steps; panning, running the sample through a Frantz Isodynamic Separator and placing the sample within Heavy Liquids. Apatite has a specific gravity of 3.16-3.22 which is greater than most minerals such as Quartz and Feldspars. Therefore panning can help separate out apatite from these minerals. The sample was panned by placing it in the black bowl found below the sink. Water was then added to the bowl and carefully tipped down the sink to remove only rock dust from the sample. Once this had been achieved the sample was panned over the top of the larger green bowl found below the sink. This ensured that panned light minerals would be transferred to the green bowl. Once panning removed most (approximately 90%) of the sample into the green bowl, these panned lights could be placed in the funnel on the sink to dry. Filter paper found in the cupboard was placed in the funnel beforehand. The panned heavy minerals which contained most of any apatite present in the sample were also placed into a funnel containing filter paper to initially dry before being placed on a hotplate to dry further before the next step. It was critical that the hotplate did not exceed ~60°C as this is the temperature at which apatite can begin to partially anneal (Wagner and Van den Haute 1992). Once the panned 'heavy' minerals from the sample had dried, a magnet was used to remove any highly magnetic minerals. Two kimwipes were placed over the magnet so those magnetic minerals could be quickly removed. Prior to use, the Frantz was cleaned using the airgun. To ensure all components of the Franz were cleaned, the Frantz track was removed my undoing the four bolts located on the side of the machine. The Franz was turned on using the on switch at the front of the machine. The remaining part of the sample was run through the Franz at 0.5 and then again at 1.4. Both the magnetic minerals and the non-magnetic minerals to be used in the next step were collected at the base of the Frantz. Heavy liquids (Geoliquid Inc. Methylene Iodide, Density: 3.32) were used to further separate out apatite grains from other minerals such as quartz and feldspars. This step was carried out within the fume cupboard at the back of the room. Dr Katherine Howard oversaw this step the first time it was carried out to ensure that all steps outlined in the lab training were carried out.

Once this step was performed, the apatite fraction was dried on a hotplate and placed into a vile using a paintbrush. The paintbrush and vial were placed in a small sealable bag which was labelled. The light minerals from the heavy liquids as well as the magnetic minerals were also placed in individual bags and labelled.

Mounting Apatite Grains (Picking): Mounting of apatite grains on to a glass slide was carried out in The University of Adelaide's Mawson Building Microscope Room (G36). Olympus SZ61 (Zoom: 6.7x-45x; Zoom Ratio: 6.7:1) microscopes were used. Picking apparatus including petri dishes and picks were cleaned using ethanol and kim-wipes followed by a visual check under the microscope. This was crucial to avoid contamination of the samples. Slides were prepared by applying double sided sticky tape. A small portion of a sample was placed onto a petri dish at a time. Apatite grains were selected based on their clear looking appearance and hexagonal shape. Once selected apatite grains were placed on to the double sided tape using a pick (using the natural oils from the skin as an adhesive) and arranged into a raster. The raster was constructed on a particular part of the slide to ensure grains could be reached by the LA-ICP-MS. Sample numbers were recorded on the slides using fine permanent marker and covered with clear tape.

Epoxy Resin: Epoxy Resin was placed on top of the apatite rasters. This was conducted in the Mawson Buildings lapidary. Gloves, labcoats and safety glasses were worn. The resin was prepared by mixing EpoxiCure™ Epoxy Resin 20-8130-032 and EpoxiCure™ Epoxy Hardener 20-8132-008 together in a plastic cup for 20 minutes. A ratio of 5:1 Resin: Hardener was achieved using scales. A popstick was used to place 1-2 small drops of the resin onto the apatite rasters. Additional glass slides were arranged on and around the original glass slide to allow a final glass slide to be placed on top of the arrangement, meaning the resin would be exactly 1 slide width thick. The resin was left for 5 days to ensure it had dried. Following this, the original glass slide and two sided tape was removed from the glass slide with resin and embedded apatite grains using a razor blade.

Grinding: Samples were ground in the Mawson Building's lapidary. Grinding reveals an internal surface within the apatite grains. Before samples were ground, the sharp edges of the glass slides were rounded off using the Zinc Lapping Disc. This was to reduce wear and tear on the polishing cloths detailed below. Samples were ground by running the slides face down in a figure eight motion. This was done initially on Waterproof Silicon Carbide Paper FEPA P# 800 followed by FEPA P# 2400. Samples were intermittently checked every 2-4 figure eight cycles under the microscope to ensure that only the tape and a small portion of the apatite grains were ground off. Large globules of tape were removed from the sample using fine tweezers.

Polishing: A Struers™ DP-U4 Cloth Lap was used to polish samples, located in the Mawson Building's lapidary. A 3µm Struers MD Dac™ polishing cloth and 1µm Struers MD Nap™ (300 mm diameter) polishing cloth were placed onto the magnetic plate and used to polish the samples. 3-6 sprays of 3µm and 1µm Diamond Suspension Polishing Lubricant was applied to the 3µm and 1µm polishing cloths before use respectively. The machine was set to 100 RPM and samples/glass slides held gently on the polishing cloths using a slide holder. Samples were intermittently checked after

every five minutes of polishing to see if scratches upon apatite grains had been removed. This was done using an Olympus BX51 microscope at 1000x magnification within the Mawson Buildings Microscope Room (G36).

Etching: Etching of samples was undertaken within the Mawson Building's B13 laboratory. Access to the room was acquired through contacting David Bruce (Email: david.bruce@adelaide.edu.au). Samples were cleaned gently with ethanol and kimwipes. All safety rules listed on the laboratory door were followed. In preparation for etching, a large bottle containing 5 mol/L Nitric acid (HNO_3), a 50ml clear plastic vile and a large beaker (approx. 2L) filled with H_2O from the sink was placed within the fume cupboard. Following this approximately 40ml of Nitric acid was poured carefully into the 50ml plastic vile from the large bottle and returned to the plastic tub it is stored in. The thermometer was used to ensure that the temperature of the plastic vile containing Nitric acid was between 19.5°C and 20.5°C. Once this was achieved by either heating using body heat from hands or cooling using the fridge, the thermometer tip was rinsed using distilled water. Slides were then chemically etched individually by submerging half the slide containing the samples into the Nitric acid for 20 seconds. The slides were then immediately placed in the beaker of water. After this process was completed, the vile containing nitric acid was poured carefully into the liquid wastes bottle and then placed in the recycling tub. The beaker of water was poured into the sink and rinsed out before being returned to the fume cupboard. The slides were removed from the water and dried using paper towel.

Track Counting & Measuring: An Olympus BX51 microscope at 1000x magnification was used to count surface fission tracks within sample grains. Before counting and measuring, samples were submerged in ethanol and dabbed dry with kim-wipes. In preparation for track counting and for the laser later on an image/map of each sample was made using the Olympus BX51 Digital Camera and handset along with Microsoft Office Word 2010. This was used for naming and identifying grains whilst using the microscope and laser. Grains that exhibited zonation or uneven distribution of tracks and features uncharacteristic of apatite were not counted. Both transmitted and reflected light was used to identify tracks. Surface fission tracks were identified as being liner features that exhibited an etch bit. The following information was recorded into a notebook; grain number, picture number, track count area, track count, grain size, grain quality. Confined track lengths were also measured using an accompanying Olympus BX51 Digital Camera and handset connected to a computer. The following information was recorded in a notebook; grain number, picture number, confined track length, angle to Dpar, 5 Dpar lengths and whether the track was a 'track in track' (TINT) or a 'track in cleavage' (TINCLE). An international standard apatite (Durango apatite) and an in-house standard (ARK 707 – Arkaroola) were counted as well for calibration purposes. In preparation for the laser an image/map of each sample was made using the Olympus BX51 Digital Camera and handset. This was used for navigation while using the laser. Pictures were taken in both reflected and transmitted light for grains counted, all confined tracks measured including Dpar lengths/angles and Dpar measurements for counted grains. This provided a future reference which was stored to a USB. This was achieved using an accompanying Olympus BX51 Digital Camera and handset connected to a computer.

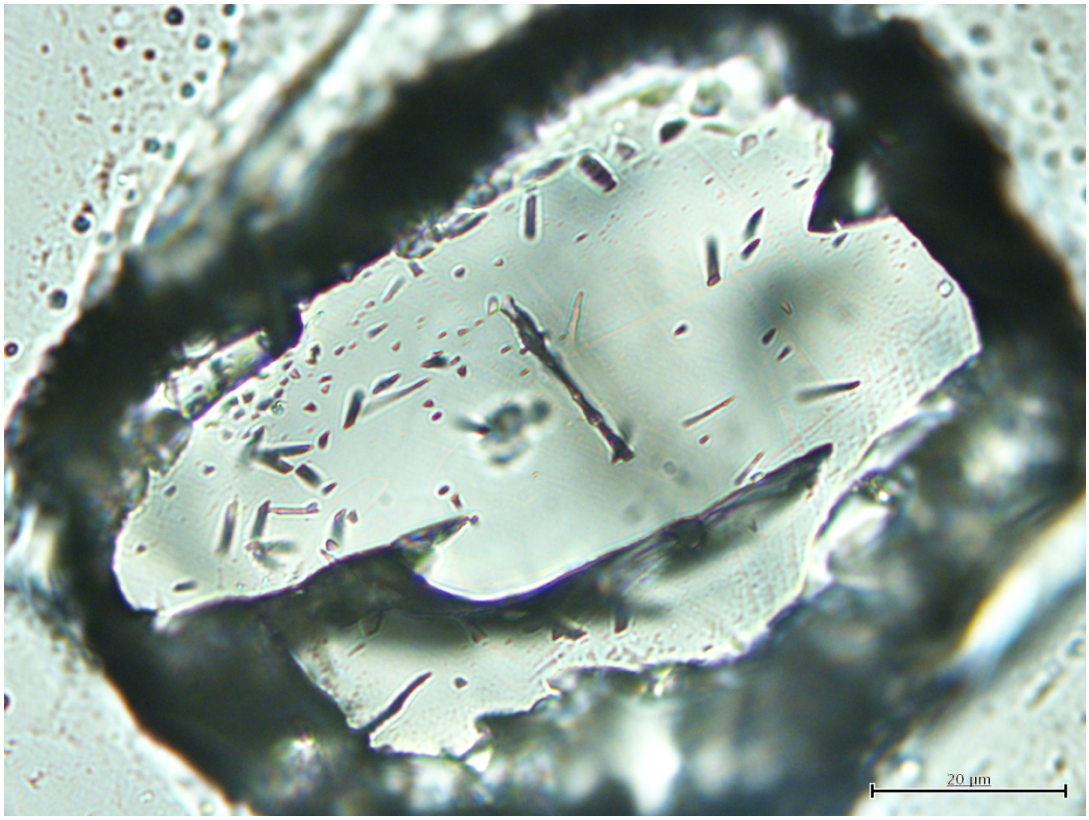

Figure 1: Example of an apatite grain from which fission tracks were counted. From sample 972.

Laser Ablation: Sample Uranium content was measured using Laser Ablation-Inductively Coupled Plasma-Mass Spectrometry (LA-ICP-MS) as opposed to conventional thermal neutron irradiation. This was carried out at The University of Adelaide's Adelaide Microscopy centre. An Agilent 7700s ICPMS coupled with Resonetics M-50-LR 193nm Excimer Laser was used. Training was conducted by Dr. Benjamin Wade (Adelaide Microscopy staff member). Procedures outlined in the user instructions booklet were followed. Analytical details for laser ablation are presented in Table 1.

Table 1: Analytical details for the LA-ICP-MS as used for apatite fission track dating.

ICPM-MS	
Brand and model	Agilent 7700s
Forward power	1300 W
Gas flows (L/min)	
Cool (Ar)	15.00
Auxiliary (Ar)	0.89
Carrier (He)	0.70
Sample (Ar)	0.93
Laser	
Type of Laser	Excimer laser

Brand and Model	Resonetics M-50-LR
Laser wavelength	193nm
Pulse duration	20 ns
Spot size	32 µm
Repetition rate	5 Hz
Energy attenuation	50%
Laser fluency	~7 J/cm^{-2}
Laser warm up (background collection)	15 s
Data acquisition parameters	
Data acquisition protocol	Time-resolved analysis
Scanned masses	235, 238, 43
Samples per peak	1
Number of scans per peak	1
Detector mode	Pulse counting
Detector deadtime	35 ns
Background collection	15 s
Ablation for age calculation	30 s
Washout	15 s
Standardisation and data reduction	
Primary standard used	NIST 610, NIST 612, NIST 614
Secondary standard used	Calibration line Durango apatite (McDowell et al. 2005)*
Data reduction software used	In-house Excel® spreadsheet

McDowell F. W., McIntosh W. C. & Farley K. A. 2005, A precise 40Ar–39Ar reference age for the Durango apatite (U–Th)/He and fission-track dating standard, *Chemical Geology* **214**, 249-263.

Data Reduction: Raw data/LAICPMS output was corrected for background signal using an in-house MS Excel® spreadsheet (average_ratios_adl_nlw.xls). Poor signals were corrected for manually or deleted if they were particularly bad. Correction was also made for grains that were zoned. The corrected output was transferred to a second in-house MS Excel® spreadsheet (ICP_datareduction_v1.2.xls). Comments on any manual correction of signals were made for each grain for future reference. AFT age calculations were built into this spreadsheet. These are based on the Grain Age Equation found in Hasebe et al. (2004).

The Age Equation is given by:

$$t = \frac{1}{\lambda_D} \ln\left(1 + \frac{\rho_s \lambda_D M}{\lambda_f N_A{}^{238}U 10^{-6} d R_{sp} k}\right)$$

Where t= FT age years, λ_D= ^{238}U total decay constant (1.55125 x 10^{-10}year^{-1}), λ_f= ^{238}U spontaneous fission decay constant (8.46 x 10^{-17}year^{-1}), N_A=Avogadro's number, ^{238}U= Uranium-238 content measured by LA-ICP-MS (µg/g), d= apatite density (taken as 3.19 g/cm^3), R_{sp} a registration factor by which ^{238}U in a unit volume would leave spontaneous tracks on an observed surface (cm), k= a constant which is variable depending on experimental factors such as etching and observation conditions, ρ_s = spontaneous fission track density at the observed surface (cm^{-2}) and M= the mass of ^{238}U.

The Error of Grain Age is given by:

$$t\sqrt{\frac{1}{N_s^2}+\delta^2}$$

Where N_s=the number of counted spontaneous tracks, and δ=uncertainties in uranium concentration (10%=0.1).

In this thesis we used a registration factor R_{sp} value of 7.25. This represents (real) Durango half lengths which we used as opposed to an average of the real half-lengths of samples in this study. This was due to half lengths being under constrained in some samples. Glorie et al. (2010) justifies the use of 7.25 for the R_{sp} value.

Dpar Measurements: In addition to track counting and confined track measuring, five etch bit (Dpar) measurements were taken for each successful grain counted following the laser and data reduction. This was done to avoid collecting data for grains which had to be deleted as a result of poor signals. An Olympus BX51 microscope at 1000x magnification with an accompanying Olympus BX51 Digital Camera and handset connected to a computer was used. Images were saved to a USB for future reference.

Modelling: Thermal histories were modelled using the software program HeFTy which uses forward and inverse modelling (Ketcham 2005). AFT and where possible AHe and ZHe data were used to perform this numerical modelling. This includes length data. Constraints were used to run the models. These constraints included a high-T start point and low-T endpoint as well as any AFT, AHe or ZHe age peaks. The software uses a Monte Carlo simulation where statistically good thermal history paths are saved. A model was deemed complete once ten good paths were obtained. If this was not possible further constraints were added to try and produce 10 good paths. Another solution was to lower the 'merit of good path' value to help obtain 10 good paths.

Apatite U-Th-Sm/He (AHe) and Zircon U-Th-Sm/He (ZHe) Thermochronology

Apatite (AHe) and Zircon (ZHe) U-Th-Sm/He low-T thermochronology is based on the diffusion of radiogenic ^{4}He through the crystal lattice at elevated temperatures (Ehlers and Farley 2003, De Grave et al. 2012). Accumulation of ^{4}He is produced in the crystal lattice by the series decay of ^{238}U, ^{235}U, ^{232}Th and by α decay of ^{147}Sm (Farley 2002). ^{4}He is partially removed when temperatures cool to a certain temperature and further cooling leads to a complete block in ^{4}He diffusion and its removal from the crystal lattice (Wolf et al. 1998). The temperature zone where ^{4}He is partially retained is called the Partial Retention Zone (PRZ) (Wolf et al. 1998). The closure temperature of radiogenic ^{4}He within apatite is ~45-75˚C, therefore this method records the time of cooling below ~45-75˚C (Ehlers and Farley 2003). By determining the concentration of ^{4}He, ^{235}U, ^{232}Th and ^{147}Sm an age by which a sample reached the closure temperature can be calculated (Farley 2002). The AHe dating method is widely used in conjunction with the AFT technique in refining time-temperature models (Ehlers and Farley 2003).For zircon, He-diffusion is blocked at much higher temperatures with a closure temperature of ~200-130˚ C (Wolfe and Stockli 2010). Therefore, the ZHe method records cooling at much higher temperatures compared with the AHe method. The ZHe method can also be used in conjunction with the AFT method to refine time-temperature models. For more information on the AHe and ZHe theory see (Ehlers and Farley 2003).

Grain selection for several samples that were selected for Apatite U-Th-Sm/He and zircon U-Th-Sm/He analysis was carried out in-house at The University of Adelaide while analysis was performed at the John de Laeter Centre for Isotope Research, Curtin University. 10-15 apatite and 8-10 zircon grains were selected for each sample in which the AHe and ZHe methods were applied. Those zircon and apatite grains which were inclusion free, exhibited a typical grain shape and were greater than 70 micrometres in size were preferentially selected. The analysis involved thermal extraction of helium using a 1064 nm Nd-YAG laser that aloud ^{4}He abundances to be determined via an Agilent 7500CS mass spectrometer. U and Th contents were determined using isotope dilution inductively coupled mass spectrometry via the Agilent 7500CS mass spectrometer. Refer to (Yu et al.) or (Li et al. 2014) for further information on the methodology specific to Curtin University. Results of this analysis were received in an Excel spreadsheet. Data from this analysis was included in to the HeFTy thermal histories models.

APPENDIX B: DATA REDUCTION INPUT

Appendix B shows the input for all samples that was used in the data reduction process. Data reduction procedures and AFT age calculations were carried out using an in-house MS Excel® spreadsheet provided by Dr. Stijn Glorie (The University of Adelaide), based on the protocols outlined in (Hasebe et al. 2004). 'Run' refers to each run carried out on the LA-ICP-MS. Data reduction was carried out separately for each run.

RUN 1

secondary standards (Durango)

Name	Drift Corr. Slope	meas 238	SD %	meas 44	SD %	meas 238/43	SD %	meas 238/44	SD %	238U Dur	RF	SD	Ns	A	rho s	t (Ma)	SD t
A1-1	2.449294	9799.838	1.017038	3033099	1.114317	0.050676	0.444906	0.003238	0.416223	10.986	0.436686	0.047973	15	10000	150000	27.27	7.04
A1-2	2.448945	9918.518	1.070589	3067516	1.082951	0.050699	0.455455	0.003237	0.423924	10.985	0.444341	0.048809	17	10000	170000	30.90	7.50
A1-3	2.443708	10303.32	0.729089	3178561	0.691684	0.050634	0.438103	0.003244	0.419356	11.031	0.449462	0.049579	21	10000	210000	37.99	8.29
A1-4	2.443359	10345.37	0.703688	3187081	0.655579	0.050529	0.37981	0.003247	0.352795	11.044	0.389195	0.042982	16	10000	160000	28.93	7.23
A1-5	2.438122	10749.78	0.90254	3329708	0.891746	0.050504	0.419822	0.003231	0.386167	11.013	0.439664	0.048419	21	10000	210000	38.05	8.31
A1-6	2.437773	10421.32	0.833627	3246059	0.807844	0.050064	0.526387	0.003214	0.447208	10.954	0.495594	0.054288	14	10000	140000	25.53	6.82
A1-7	2.432536	10763.58	0.918643	3360901	0.834863	0.050033	0.443145	0.003203	0.405272	10.942	0.485691	0.053143	18	10000	180000	32.84	7.74
A1-8	2.432187	10243.83	0.830295	3181819	0.81442	0.050425	0.451431	0.003222	0.421737	11.010	0.501544	0.055217	17	10000	170000	30.83	7.48
A1-9	2.42695	10730.38	0.805622	3387644	0.705116	0.04923	0.433352	0.003167	0.388227	10.845	0.509332	0.055237	13	10000	130000	23.95	6.64
A1-10	2.426601	10749.75	0.716234	3332929	0.707964	0.050525	0.454121	0.003228	0.405287	11.055	0.524969	0.058035	22	10000	220000	39.71	8.47
A2-1	2.421364	7534.044	0.807045	3177309	0.726175	0.03703	0.507179	0.002373	0.47985	8.143	0.621058	0.050573	20	10000	200000	48.97	10.95
A2-2	2.421015	7145.297	0.861768	3077010	0.785537	0.036168	0.486253	0.002324	0.475315	7.976	0.620186	0.049463	16	10000	160000	40.03	10.01
A2-4	2.415429	7084.079	0.791793	3065005	0.82965	0.036274	0.568993	0.002316	0.51172	7.968	0.69122	0.055077	14	10000	140000	35.07	9.38
										10.304	0.508	0.051	17.231	130000	172308	33.85	8.14
													224			**33.38**	2.24

Unknowns (samples)

Name	Drift Corr. Slope	meas 238	SD %	meas 44	SD %	meas 238/43	SD %	meas 238/44	SD %	Dur	RF	SD	Ns	A	rho s	t (Ma)	SD t
9594 A5	2.448596	6569.372	3.961072	4267244	3.668744	0.023629	1.292122	0.001511	1.275499	5.068	1.28255	0.064995	34	3000	1133333	432.76	74.43
9594 A8	2.448247	4463.201	1.144799	5315174	0.802296	0.013205	1.260875	0.000843	1.255897	2.827	1.263194	0.035714	20	1800	1111111	742.16	166.22
9594 B6	2.447898	8383.366	2.317888	5253862	1.845547	0.024973	1.581142	0.001599	1.580501	5.363	1.586426	0.085077	25	2400	1041667	377.50	75.74
9594 B7	2.447548	5054.786	2.676408	4959096	1.008638	0.015657	1.81769	0.001004	1.801795	3.366	1.80711	0.06083	14	1600	875000	500.34	134.03
9594 B11	2.447199	8030.189	2.301747	5423406	1.562929	0.023063	1.240441	0.001471	1.226818	4.935	1.234794	0.060934	28	2100	1333333	519.30	98.35

9594 C1	2.44685	9767.616	1.094529	6077608	0.817702	0.025343	0.808683	0.001607	0.742467	5.393	0.755896	0.040765	31	2100	1476190	525.82	94.52
9594 C7	2.446501	6672.928	2.819685	4661650	1.029397	0.022563	2.890827	0.001438	2.866746	4.825	2.870345	0.138507	29	2000	1450000	575.01	108.04
9594 D1	2.446152	7484.395	1.00646	5628494	1.146257	0.020963	0.683189	0.001335	0.679475	4.479	0.694907	0.031126	75	5600	1339286	572.29	66.20
9594 D4	2.44301	4319.064	1.633058	4887380	1.050857	0.01378	0.941126	0.00088	0.93114	2.958	0.946001	0.02798	22	3500	628571.4	411.91	87.91
9594 D9	2.442661	7874.955	1.738755	4841183	1.104646	0.025388	0.991838	0.001618	0.952769	5.438	0.967776	0.052631	41	4000	1025000	366.61	57.37
9594 E9	2.442312	5950.522	2.716258	4879207	2.687962	0.019226	1.270049	0.001227	1.265244	4.125	1.27696	0.052678	19	2400	791666.7	373.09	85.73
9594 E14	2.441962	7152.455	0.910118	5596366	0.961686	0.02013	0.684839	0.00128	0.696959	4.304	0.718703	0.030936	7	900	777777.8	351.87	133.02
9594 F10	2.441613	4285.598	2.754063	4843391	1.158302	0.013673	1.960596	0.000874	1.889151	2.939	1.897553	0.055766	37	3500	1057143	682.53	112.95
9594 F11	2.441264	14327.19	1.713946	5372109	0.871008	0.041843	1.310602	0.002663	1.235415	8.955	1.248654	0.111822	56	5000	1120000	245.58	32.96
9594 G10	2.440915	7987.619	1.495406	4813816	1.192451	0.025974	0.868453	0.00166	0.864661	5.583	0.884101	0.049358	23	2800	821428.6	287.96	60.10
9594 H4	2.440566	11230.27	1.000791	5295635	0.867596	0.033503	0.501303	0.00212	0.460832	7.133	0.4975	0.035487	33	2500	1320000	360.14	62.72
9594 H5	2.437424	9000.108	1.45579	4961328	1.258437	0.028465	0.607315	0.001812	0.562237	6.104	0.602664	0.036785	32	3000	1066667	340.61	60.25
9594 I5	2.437075	4634.169	1.5534	4916769	1.420439	0.014788	0.834661	0.000943	0.806028	3.177	0.835636	0.026544	16	3500	457142.9	281.79	70.49
9594 I6	2.436725	12390.68	0.957546	5561492	0.826401	0.035188	0.626209	0.002229	0.596569	7.509	0.637222	0.04785	33	1800	1833333	471.02	82.05
965 B4	2.436027	36441.69	1.271605	5966508	0.81208	0.095845	0.638499	0.006086	0.642347	20.510	0.682625	0.140009	159	4200	3785714	359.23	28.59
965 C5	2.435678	57632.91	1.839874	5915331	1.844484	0.152806	0.305562	0.009745	0.289582	32.847	0.372673	0.122411	75	2400	3125000	187.66	21.68
965 D1	2.435329	50854.86	2.388483	5779831	1.644535	0.136653	0.859781	0.008688	0.80032	29.288	0.835007	0.244554	157	2500	6280000	415.49	33.34
965 F1	2.43498	66804.91	1.236685	6092534	1.217786	0.172894	0.28207	0.010967	0.262799	36.978	0.357105	0.132049	113	2000	5650000	298.79	28.13
965 F3	2.431838	42544.39	1.067485	7322490	0.916611	0.092027	0.988034	0.00582	0.904874	19.648	0.945808	0.185835	126	2800	4500000	442.83	39.67
965 F6	2.431489	61360.86	1.026033	5918443	0.769672	0.16293	0.720887	0.010369	0.724672	35.010	0.776539	0.271866	178	3600	4944444	276.65	20.85
965 G8	2.431139	63419.58	1.133674	6040336	1.276589	0.165843	0.296397	0.010524	0.282411	35.539	0.399706	0.142051	161	3000	5366667	295.37	23.31
965 H7	2.430441	103343	1.227801	6535299	1.354924	0.250001	0.342054	0.015854	0.325794	53.553	0.436527	0.233774	102	1600	6375000	233.96	23.19
965 I1	2.430092	85730.04	0.728201	6705416	0.883733	0.201256	0.389747	0.012798	0.347587	43.238	0.45551	0.196952	159	2400	6625000	299.60	23.80
965 I7	2.429743	75528.85	0.687176	6573610	1.055003	0.181753	0.62405	0.011555	0.614301	39.044	0.682887	0.266629	159	2800	5678571	284.71	22.66
965 I8	2.429394	44780.16	0.827214	6171011	0.640601	0.114137	0.570163	0.007256	0.480167	24.520	0.56733	0.139108	127	2400	5291667	418.09	37.18
965 J1	2.426252	61212.74	2.205172	5047591	1.874846	0.191005	1.347312	0.012123	1.314333	41.022	1.357012	0.556676	125	2000	6250000	297.95	26.95
965 J3	2.425903	54105.95	1.339144	6271521	0.818915	0.13744	1.683997	0.008725	1.706543	29.529	1.740406	0.513924	52	2400	2166667	145.21	20.30
965 J6	2.425553	78393.8	0.843815	7059656	0.750376	0.175799	1.114546	0.011176	1.134115	37.828	1.185618	0.448498	154	2500	6160000	317.95	25.90

965 J7	2.425204	57665.51	1.606441	5988683	0.687233	0.153317	1.955564	0.009722	1.952243	32.912	1.983309	0.652746	90	2500	3600000	215.29	23.09
965 K8	2.424855	104511.7	0.585521	6166277	1.076495	0.269637	0.892657	0.017097	0.876429	57.884	0.945101	0.547064	83	1600	5187500	176.92	19.49
965 K9	2.424506	36166.2	1.683385	5765793	0.812465	0.099298	1.646708	0.006296	1.671333	21.321	1.709183	0.36441	45	2400	1875000	173.66	26.06
116 B3	2.424157	55638.36	3.834989	5383537	1.075928	0.159405	3.052271	0.01013	3.072849	34.307	3.094068	1.061482	100	1200	8333333	468.71	49.06
116 C2	2.423808	60493.66	1.80149	5674199	1.106783	0.167149	0.980231	0.010623	0.984096	35.984	1.049877	0.377783	78	1500	5200000	282.94	32.17
116 C9	2.420317	28963.83	0.746036	4712027	0.93187	0.096636	0.47805	0.00616	0.494569	20.895	0.640246	0.133782	57	1500	3800000	354.08	46.95
116 C10	2.419967	49360.15	5.595621	3577108	5.505797	0.205976	1.551656	0.01312	1.568204	44.510	1.621094	0.721545	48	900	5333333	235.47	34.20
116 D2	2.419618	50963.28	1.87762	4958729	1.004319	0.160564	1.030412	0.010209	1.01493	34.639	1.096433	0.379795	68	900	7555556	422.42	51.44
116 D3	2.419269	26771.94	1.047977	5208053	1.318139	0.081516	0.770724	0.005182	0.793975	17.584	0.89773	0.15786	17	1200	1416667	159.26	38.65
116 E4	2.418571	73673.2	1.419344	5295449	1.499712	0.219125	0.507174	0.013937	0.470656	47.308	0.635639	0.300711	80	1600	5000000	208.14	23.31
116 E7	2.418222	29004.64	2.267865	5284305	1.528546	0.086406	1.84221	0.005493	1.812456	18.650	1.863082	0.34747	124	1600	7750000	782.26	71.75
116 F4	2.41508	24066.82	2.944103	5047333	1.076223	0.073236	2.112868	0.004668	2.060227	15.868	2.112905	0.335268	87	1800	4833333	582.53	63.66
116 F7	2.41473	48174.26	1.768703	5342297	1.410347	0.141684	1.062626	0.00897	1.016332	30.498	1.121031	0.341891	60	900	6666667	423.31	54.85
116 G7	2.414381	36362.13	1.629689	5464898	1.069255	0.105032	1.136139	0.006645	1.068029	22.597	1.169808	0.264337	131	2800	4678571	401.63	35.40
116 H2	2.414032	23503.84	0.771798	5370545	0.706159	0.068987	0.820665	0.004391	0.820328	14.934	0.951171	0.142051	102	1500	6800000	852.41	84.79
116 I2	2.413683	38247	0.746152	5616509	0.613377	0.107746	0.455652	0.00681	0.426135	23.165	0.646098	0.149666	87	1600	5437500	453.48	48.71
116 I10	2.413334	31861.82	4.091847	3700426	3.250158	0.128433	1.837426	0.008189	1.806458	27.857	1.871696	0.521405	82	1800	4555556	319.27	35.76
116 J2	2.412985	26393.68	3.108212	5137811	1.973555	0.079229	1.722486	0.005038	1.673276	17.141	1.744692	0.29906	37	900	4111111	463.00	76.54
116 J8	2.412636	37741.83	1.706586	5332692	1.606048	0.111329	0.550318	0.007075	0.531181	24.075	0.728306	0.175342	112	1200	9333333	732.67	69.44
									Sample 1	4.973	1.158	0.055	30.263	53500	1074766	443.07	87.53
										238U Dur	RF	STD	575			**418.69**	**18.07**
									Sample 2	34.745	0.908	0.303	121.471	43100	4791183	284.67	26.13
										238U Dur	RF	STD	2065			**270.25**	**6.40**
									Sample 3	26.876	1.328	0.357	79.375	22900	5545852	446.35	51.04
										238U Dur	RF	STD	1270			**400.32**	**12.43**

RUN 2

Secondary standards (Durango)

Name	Drift Corr. Slope	meas 238	SD %	meas 44	SD %	meas 238/43	SD %	meas 238/44	SD %	238U Dur	RF	SD	Ns	A	rho s	t (Ma)	SD t
A3 1	1.786139	40850.42	1.100172	14810560	1.323964	0.04336	0.652794	0.002765	0.557287	12.864	0.844821	0.108675	14	10000	140000	21.75	5.81
A3 2	1.785205	40900.31	1.020258	14798338	1.18338	0.04371	0.587603	0.002769	0.543581	12.889	0.836384	0.107801	15	10000	150000	23.25	6.01
A3 3	1.771197	39272.74	1.047987	14367242	1.263404	0.043316	0.657115	0.00274	0.610087	12.856	0.893218	0.114834	16	10000	160000	24.86	6.22
A3 4	1.770263	36836.2	1.257616	13347517	1.478785	0.044074	0.790623	0.00277	0.738993	13.003	0.986776	0.12831	16	10000	160000	24.58	6.15
A3 5	1.756255	37182.69	0.922527	13699228	1.029665	0.043644	0.535025	0.002718	0.535125	12.860	0.867271	0.111532	21	10000	210000	32.60	7.12
A3 6	1.755321	38068.78	0.737075	14024161	0.906026	0.043468	0.665264	0.002719	0.591686	12.870	0.904992	0.116473	14	10000	140000	21.74	5.81
A3 7	1.741313	36681.36	0.931641	13822505	1.115475	0.043085	0.716369	0.00266	0.752773	12.695	1.044617	0.132617	13	10000	130000	20.46	5.68
A3 8	1.74038	36967.85	1.234207	13629538	1.387852	0.044129	0.70024	0.00272	0.659533	12.985	0.98176	0.127485	15	10000	150000	23.08	5.96
A3 9	1.726372	38909.02	1.210298	13458750	1.226024	0.047184	0.77394	0.002895	0.685496	13.935	1.035744	0.144331	14	10000	140000	20.08	5.37
A3 10	1.725438	35858.53	1.015183	13158071	1.009439	0.043749	0.691138	0.002728	0.613123	13.137	0.992141	0.13034	11	10000	110000	16.74	5.05
A4 1	1.71143	22412.57	1.040806	13502676	1.254532	0.026961	0.651766	0.001664	0.699118	8.081	1.091087	0.088165	11	10000	110000	27.19	8.20
A4 2	1.710496	22125.71	0.916921	13507931	1.062531	0.026358	0.683182	0.00164	0.581921	7.969	1.023338	0.081552	14	10000	140000	35.07	9.38
A4 3	1.696488	20844.88	0.796192	12744587	0.894199	0.026709	0.738316	0.001638	0.702255	8.026	1.146871	0.092043	14	10000	140000	34.82	9.31
A4 4	1.695554	21435	0.997276	13183128	1.244362	0.026419	0.616731	0.00163	0.608696	7.987	1.09587	0.087527	15	10000	150000	37.48	9.69
A4 5	1.681546	21268.94	1.093781	13185541	1.279346	0.026261	0.796647	0.001618	0.693736	7.993	1.202736	0.09614	7	10000	70000	17.50	6.62
A4 6	1.680613	21686.02	0.93878	13144426	1.043116	0.026772	0.794895	0.001653	0.700312	8.172	1.210565	0.098921	10	10000	100000	24.45	7.74
A4 7	1.666605	21329.59	0.890686	13148463	0.962376	0.026498	0.594312	0.001624	0.614627	8.099	1.228862	0.099521	14	10000	140000	34.51	9.23
A4 8	1.665671	20212.12	1.316243	12661039	1.672918	0.026244	0.934787	0.001605	0.796741	8.007	1.333563	0.106783	18	10000	180000	44.84	10.58
A4 9	1.651663	22113.14	1.504892	12887105	1.671909	0.028397	0.873985	0.001722	0.682607	8.662	1.338068	0.115898	10	10000	100000	23.07	7.30
A4 10	1.650729	22870.81	0.80097	13363032	0.86468	0.028114	0.701444	0.001714	0.712159	8.629	1.358129	0.11719	19	10000	190000	43.92	10.09
										10.586	1.070841	0.110307	14.05	200000	140500	27.60	7.37
													281			**26.51**	1.61

Unknowns (samples)

Name	Drift Corr. Slope	meas 238	SD %	meas 44	SD %	meas 238/43	SD %	meas 238/44	SD %	238U Dur	RF	SD	Ns	A	rho s	t (Ma)	SD t
967 B11	1.784271	6793.498	4.58574	2816966	6.198864	0.036521	3.274623	0.002479	4.314284	11.405	4.360971	0.497358	27	2100	1285714	221.78	43.76
967 C6	1.783337	5045.958	2.80249	3423289	2.924543	0.023191	2.552848	0.001484	2.735167	6.833	2.808416	0.191908	54	2800	1928571	541.49	75.24
967 C10	1.782403	3067.043	2.402493	2876561	2.340124	0.016273	1.835884	0.001073	1.712721	4.944	1.827725	0.090355	37	3600	1027778	403.23	66.70
967 D1	1.781469	3035.362	1.246075	3151073	1.120597	0.015031	1.442299	0.000967	1.350795	4.455	1.494316	0.066577	18	1800	1000000	434.27	102.56
967 D11	1.780536	3840.502	1.786923	2818972	2.224187	0.020645	1.962947	0.001382	1.740682	6.373	1.8546	0.118203	84	5400	1555556	470.87	52.11
967 E1	1.779602	9551.62	2.273539	3124569	1.370516	0.04747	1.748437	0.003056	1.728272	14.098	1.843311	0.259874	72	2400	3000000	412.43	49.20
967 E2	1.778668	1467.075	2.141182	2815100	1.564599	0.008193	1.958849	0.000523	1.833438	2.415	1.94261	0.046923	28	4000	700000	555.40	105.51
967 E11	1.777734	4443.97	1.076737	2685900	1.152851	0.024669	1.38769	0.001663	1.379859	7.680	1.522395	0.116914	64	3000	2133333	533.32	67.16
967 F2	1.769329	3901.81	1.596299	3167585	1.509661	0.019215	0.979407	0.001233	0.927448	5.724	1.135706	0.065003	58	3600	1611111	540.13	71.19
967 F4	1.768395	24049.4	1.669681	3563631	1.712591	0.104401	0.935931	0.006762	1.110106	31.393	1.29001	0.404974	140	4000	3500000	219.37	18.75
967 G1	1.767462	6308.055	2.586639	3374560	2.017721	0.029213	1.407957	0.001869	1.46025	8.682	1.601971	0.139087	56	3600	1555556	348.98	46.97
967 G2	1.766528	4972.457	2.139256	3314475	1.99024	0.023375	1.408284	0.001504	1.484332	6.992	1.62465	0.113591	37	2400	1541667	426.88	70.52
967 G7	1.765594	2919.974	1.635452	2711939	1.332091	0.016169	1.581959	0.00108	1.517863	5.021	1.656045	0.083157	49	4000	1225000	470.66	67.69
967 G8	1.76466	7006.481	1.872477	2769919	2.129099	0.039606	2.303966	0.002562	1.852253	11.920	1.967693	0.23454	109	5000	2180000	356.04	34.81
967 G9	1.763726	3944.327	1.185651	2783575	1.332067	0.021272	1.471527	0.001425	1.366625	6.632	1.520235	0.100825	94	6000	1566667	456.26	47.57
967 H1	1.762792	6767.104	1.259695	3584435	1.309569	0.029652	0.886504	0.00189	0.707044	8.801	0.972576	0.085594	73	4900	1489796	330.21	38.78
967 H4	1.754388	9637.853	1.655634	3302363	1.765917	0.04513	0.810617	0.002931	0.852266	13.715	1.094745	0.150146	73	3200	2281250	324.60	38.16
967 H6	1.753454	2391.014	3.612475	2626044	2.638018	0.013683	2.413277	0.00091	2.402392	4.259	2.499372	0.106456	64	4800	1333333	597.94	76.22
967 I1	1.75252	2893.742	1.278391	3468756	1.770221	0.013154	1.363965	0.000842	1.455654	3.944	1.61172	0.063565	21	2100	1000000	488.50	106.89
967 I3	1.751586	7758.551	2.690335	3528428	2.018054	0.034456	1.675678	0.002197	1.670483	10.298	1.809042	0.186302	197	8000	2462500	461.66	33.94
967 I5	1.750652	4495.417	1.525493	2977467	1.467863	0.022974	2.191727	0.001531	2.569747	7.180	2.662556	0.191158	90	4200	2142857	571.30	62.11
967 J1	1.748784	9155.529	5.18213	3256493	5.298739	0.04402	1.094817	0.00282	1.159786	13.237	1.355692	0.179448	59	2500	2360000	347.33	45.46
967 J2	1.74785	4662.761	1.430908	3766862	1.728573	0.019596	1.203351	0.001243	1.177612	5.841	1.372324	0.080155	37	2500	1480000	488.20	80.54
967 J4	1.739446	11542.32	0.740003	3343908	1.361254	0.053753	1.03781	0.003473	1.097728	16.390	1.318433	0.216092	50	2000	2500000	298.28	42.37
967 J10	1.738512	5546.384	1.618885	2612039	1.83896	0.032326	1.735532	0.00214	1.680207	10.106	1.833254	0.18526	51	2400	2125000	407.71	57.58

126 A7	1.737578	2793.293	7.786608	1923192	6.932416	0.0223	3.698388	0.001427	3.328522	6.742	3.409006	0.229819	54	1800	3000000	834.28	117.04
126 B3	1.736644	7734.052	1.858167	3506601	1.391508	0.034285	1.731044	0.00221	1.723067	10.446	1.875058	0.19587	62	1200	5166667	920.92	118.22
126 B4	1.73571	5325.186	1.642499	3044983	1.700926	0.027348	1.277778	0.001756	1.097932	8.307	1.325531	0.110115	35	1200	2916667	667.00	113.09
126 B5	1.734776	6980.901	2.831655	3094524	1.664987	0.035281	2.505709	0.002259	2.31792	10.690	2.434975	0.260298	58	2000	2900000	521.31	69.62
126 B7 (a)	1.733843	3951.175	1.662414	2936934	1.417903	0.02102	0.96801	0.001346	0.909386	6.373	1.178213	0.075087	45	2500	1800000	541.88	81.03
126 B7 (b)	1.732909	4173.803	1.764359	2964531	1.377357	0.021884	1.04976	0.001408	1.04098	6.669	1.284435	0.08566	15	900	1666667	481.74	124.54
126 D2	1.72357	3455.945	3.277028	3374790	3.951896	0.016472	1.54314	0.001043	1.808688	4.968	1.972599	0.097996	45	1500	3000000	1107.78	166.58
126 E6	1.722636	6080.674	4.753716	3135220	1.404477	0.029603	3.638098	0.001903	3.676768	9.068	3.760882	0.341046	73	1600	4562500	935.70	115.03
126 G5	1.721702	13235.16	4.196417	3364985	1.754835	0.060727	3.300691	0.003881	3.237435	18.508	3.333539	0.616972	82	1800	4555556	474.73	54.76
972 A2	1.720769	16203.3	2.422783	3506487	1.824771	0.072674	1.960168	0.004645	2.128804	22.161	2.273603	0.503847	44	900	4888889	427.09	65.11
972 E9	1.719835	3748.236	2.080427	3280212	2.003352	0.017656	1.617335	0.001151	1.846548	5.493	2.01327	0.11058	36	1800	2000000	690.47	115.91
972 G5	1.709562	12036.6	3.300474	3267117	2.56299	0.056166	2.164204	0.003685	2.065859	17.696	2.232338	0.395032	23	1200	1916667	213.22	44.71
972 G9	1.707694	19695.39	2.045177	2824129	2.406623	0.102752	2.035747	0.007056	2.194871	33.923	2.355251	0.798982	51	1600	3187500	185.37	26.32
972 G12	1.706761	4410.831	9.869084	3526271	1.749689	0.020122	11.38689	0.001285	11.52647	6.181	11.55839	0.714384	40	2000	2000000	617.16	120.87
972 H2	1.705827	17459.56	3.603832	3829728	3.361551	0.074002	1.172598	0.004558	1.072699	21.937	1.376578	0.301981	59	2000	2950000	263.68	34.52
972 I10	1.693687	3655.952	7.286465	3697810	2.148071	0.015413	5.894822	0.00097	5.816044	4.700	5.888429	0.276755	13	1200	1083333	445.58	126.34
972 I12	1.692753	6986.226	4.105725	3913105	2.816075	0.028781	2.380445	0.001775	2.414806	8.610	2.585933	0.222647	32	2000	1600000	361.61	64.60
972 K2	1.691819	1099.204	2.721634	3252890	2.017859	0.005309	2.165304	0.000339	2.045687	1.646	2.247048	0.036979	21	2800	750000	853.13	187.15
972 K8	1.690885	17470.37	1.535908	3283119	1.628569	0.083227	0.854103	0.005334	0.919278	25.898	1.310794	0.339463	74	1800	4111111	310.15	36.28
972 K9	1.689951	3264.156	3.424787	3519381	1.680516	0.01467	3.193242	0.000929	3.094599	4.511	3.233954	0.145895	24	1800	1333333	565.96	116.97
972 L3	1.689017	5654.114	1.657086	3067653	1.332424	0.028579	1.04772	0.001843	1.009596	8.959	1.382064	0.123826	40	2400	1666667	361.97	57.45
972 L4	1.688083	8959.619	3.837946	3138990	1.625139	0.043999	3.445387	0.002827	3.463157	13.751	3.590719	0.493745	56	3000	1866667	266.14	36.83
972 M1	1.679679	9973.112	1.034494	3276014	1.364467	0.047588	1.17582	0.00306	1.162486	14.957	1.528472	0.228609	44	1600	2750000	357.88	54.23
972 M2	1.678745	6940.008	2.113747	3124932	1.757077	0.034623	1.125837	0.002216	1.163188	10.838	1.532244	0.166065	87	3200	2718750	483.49	52.36
972 M8	1.676877	11834.92	6.585102	3602101	1.992547	0.050358	5.321764	0.004472	5.074535	21.893	5.173566	1.132667	32	1200	2666667	239.29	44.08
127 A1	1.675009	22654.77	0.961402	3974818	1.206599	0.092713	0.653025	0.005713	0.832786	28.000	1.314877	0.368166	41	900	4555556	317.68	49.79
127 A5	1.674076	7364.885	3.206337	3654532	1.830802	0.032353	3.450112	0.002024	2.986654	9.927	3.156875	0.31339	48	1600	3000000	578.13	85.42
127 A7	1.673142	24817.79	1.447687	3925842	1.864572	0.102854	1.402226	0.006357	1.54126	31.191	1.852492	0.577814	52	900	5777778	360.48	50.43

127 B12	1.664737	11445.5	4.600914	3474997	4.376812	0.053807	2.802426	0.003322	2.993831	16.383	3.180877	0.521117	32	900	3555556	420.37	75.51
127 C5	1.663803	5400.888	1.307245	3271831	1.432003	0.02497	1.41616	0.001661	1.695612	8.198	2.01035	0.164814	38	2500	1520000	360.80	58.98
127 C6	1.662869	2002.855	1.647808	3128312	1.389355	0.009629	1.919881	0.000643	1.560099	3.176	1.900493	0.060365	9	1200	750000	456.08	152.27
127 D2	1.661001	2475.348	1.346094	3822014	1.152619	0.010484	1.390228	0.00065	1.742505	3.214	2.058568	0.066172	18	2400	750000	450.85	106.67
127 E9	1.660068	6547.249	1.747673	3286485	2.333524	0.031161	1.906363	0.002018	2.127616	9.979	2.395825	0.23907	26	1800	1444444	283.40	55.99
127 G3	1.659134	3628.717	1.087088	3573854	1.443263	0.016141	1.241962	0.001023	1.412142	5.061	1.79425	0.090799	26	2100	1238095	471.97	92.95
127 G5	1.660068	5385.165	1.413251	3392838	1.525025	0.024677	1.095825	0.001593	1.212403	7.878	1.638033	0.129043	25	1500	1666667	410.11	82.30
127 H9	1.649795	2515.668	3.088849	3186371	2.019361	0.012103	2.135045	0.000791	2.700917	3.935	2.940284	0.115694	27	3000	900000	442.27	86.10
127 I10	1.648861	2577.223	1.500707	3453348	1.689763	0.011833	1.974328	0.000755	2.001162	3.760	2.316905	0.087114	18	1600	1125000	572.66	135.63
127 K6	1.646994	5518.876	1.332033	3837957	1.447949	0.023249	1.534272	0.001448	1.635257	7.220	2.01592	0.145558	15	1200	1250000	337.51	87.41
127 L3	1.64606	13073.28	0.605939	3697444	1.498333	0.057125	1.309101	0.003574	1.625056	17.823	2.010987	0.358427	42	800	5250000	564.13	87.78
127 L5	1.645126	11591.25	1.676844	3611816	1.758599	0.050873	1.363514	0.003231	1.619043	16.126	2.009492	0.324055	43	1200	3583333	430.07	66.15
127 L7	1.644192	2690.213	3.032331	1886272	1.877928	0.022002	1.513943	0.001413	1.454888	7.057	1.883365	0.132902	19	1200	1583333	434.13	99.93
									Sample 1	9.134	1.799	0.159	65.680	90300	1818383	428.27	60.68673
										238U Dur	RF	STD	1642			**386.65**	**11.68**
									Sample 2	9.086	2.286	0.224	52.111	14500	3234483	720.59	89.3122
										238U Dur	RF	STD	469			**675.83**	**35.36**
									Sample 3	13.947	3.143	0.374	42.250	30500	2216393	415.14	71.62241
										238U Dur	RF	STD	676			**310.47**	**14.56**
									Sample 4	11.183	2.155	0.231	29.9375	24800	1931452	430.6668	85.83226
										238U Dur	RF	STD	479			**336.73**	**16.88**

RUN 3

Secondary standards (Durango)

Name	Drift Corr. Slope	meas 238	SD %	meas 44	SD %	meas 238/43	SD %	meas 238/44	SD %	238U Dur	RF	SD	Ns	A	rho s	t (Ma)	SD t
DUR A2 5	1.899874	5394.405	1.348947	2752054	1.521814	0.030684	0.951038	0.001971	0.866353	8.621	0.891052	0.07682	21	10000	210000	48.57	10.61
DUR A2 6	1.899652	5067.127	1.616028	2688656	1.748143	0.029465	0.900424	0.001895	0.863374	8.291	0.888294	0.073648	13	10000	130000	31.31	8.69
DUR A2 7	1.896325	5434.186	1.295446	2827868	1.632267	0.030108	1.189769	0.001941	1.163859	8.505	1.185639	0.100833	19	10000	190000	44.56	10.24
DUR A2 8	1.896103	5257.363	2.012492	2844173	1.959766	0.029058	0.882072	0.001852	0.819256	8.118	0.850359	0.069032	14	10000	140000	34.42	9.21
DUR A2 9	1.892776	5106.489	0.898287	2919115	0.632029	0.027161	0.88402	0.001752	0.902685	7.690	0.939139	0.072215	20	10000	200000	51.85	11.60
DUR A2 10	1.892554	5105.056	1.418648	2911986	1.481606	0.027643	0.990395	0.00176	0.983298	7.728	1.017491	0.078637	21	10000	210000	54.16	11.83
										8.384	0.961996	0.078531	18	40000	167500	44.14	10.36
													67			**39.86**	4.88

Unknowns (samples)

Using alternative Zeta

Name	Drift Corr. Slope	meas 238	SD %	meas 44	SD %	meas 238/43	SD %	meas 238/44	SD %	238U Dur	RF	SD	Ns	A	rho s	t (Ma)	SD t
952 A1	1.89943	3537.561	1.198633	2508362	1.22805	0.02143	1.208525	0.001416	1.23067	6.118	1.24839	0.076382	33	2400	1375000	345.10	60.23
952 A3	1.899208	3145.761	3.7059	2339467	1.851315	0.021556	4.751003	0.001375	4.623825	5.944	4.628607	0.27512	61	4900	1244898	322.20	43.87
952 A4	1.898987	2069.426	1.576324	2261419	1.026733	0.013738	1.709341	0.000919	1.623347	3.971	1.637021	0.065009	70	4000	1750000	660.16	79.64
952 A5	1.898765	3557.942	2.625822	3097396	1.418627	0.018354	4.013384	0.001189	3.873971	5.142	3.879769	0.199495	82	4200	1952381	572.75	67.04
952 A11	1.898543	5017.25	0.991819	3285487	1.437105	0.024045	1.512196	0.001545	1.482198	6.683	1.497422	0.10007	91	6000	1516667	348.42	36.90
952 B1	1.898321	4057.393	3.024079	2252331	0.879727	0.026024	3.177206	0.001806	3.090945	7.809	3.098345	0.241964	59	3600	1638889	322.83	43.20
952 B2	1.898099	4020.882	1.170409	2341472	1.116785	0.02564	1.454518	0.001729	1.464645	7.478	1.480356	0.110701	117	4800	2437500	494.71	46.32
952 B6	1.895881	4977.362	1.249048	2125967	1.422863	0.035001	1.459813	0.002366	1.563924	10.247	1.580689	0.161972	123	4000	3075000	456.81	41.82
952 B11	1.895437	2345.59	1.997338	3340612	1.5267	0.011254	3.452982	0.000726	3.405401	3.143	3.413378	0.107289	64	6000	1066667	514.26	66.64
952 C11	1.895216	2095.696	2.549725	2990542	1.741215	0.01079	1.2639	0.000696	1.283854	3.017	1.305204	0.039375	44	4200	1047619	525.76	79.56
952 D4	1.894994	1802.469	1.726092	2766870	0.961096	0.009785	1.857306	0.000653	1.662784	2.828	1.679597	0.047506	49	4200	1166667	619.89	89.17

952 D8	1.894772	4932.024	1.779116	2678118	1.166784	0.027677	1.328795	0.001842	1.392488	7.981	1.412857	0.112764	77	4000	1925000	369.67	42.45
952 D11	1.89455	4524.075	1.446638	3223066	1.527011	0.022158	2.341253	0.001422	2.495178	6.163	2.506799	0.154501	55	4000	1375000	342.66	47.00
952 E2	1.894328	3959.008	1.316198	2174998	0.920795	0.02657	1.709877	0.001824	1.252778	7.905	1.276163	0.100886	136	5400	2518519	483.93	41.95
952 E4	1.892332	2095.237	4.625301	2409534	2.068341	0.01252	4.684278	0.000875	4.638509	3.796	4.646018	0.17635	47	6000	783333.3	317.59	48.62
952 F9	1.891888	4143.87	2.270621	1624288	3.301446	0.038512	2.514661	0.002611	2.753199	11.332	2.766321	0.313481	62	3200	1937500	264.22	34.34
952 F11	1.891667	5575.866	2.115313	2365343	1.762982	0.03527	2.630837	0.002396	2.372714	10.399	2.388221	0.248351	77	2800	2750000	404.22	47.07
952 G4	1.891445	1419.646	1.506236	2687490	1.113753	0.007932	1.761256	0.000532	1.685992	2.307	1.708166	0.039409	76	10000	760000	499.76	57.96
952 G11	1.891001	1128.432	1.421824	1699868	1.420526	0.009921	2.058357	0.000672	1.872269	2.916	1.893046	0.05521	57	7000	814285.7	426.04	57.00
952 J11	1.890779	4417.081	2.183054	2515539	2.41113	0.025581	3.065452	0.00177	2.859125	7.686	2.87304	0.22083	76	4000	1900000	378.60	44.77
952 K6	1.888783	2678.813	1.324582	2576925	1.031854	0.015176	1.548574	0.001044	1.383002	4.538	1.416939	0.0643	75	4000	1875000	620.90	72.23
111 A	1.888561	32284.67	2.815784	3269795	2.051372	0.150485	1.09205	0.009856	1.179787	42.847	1.220156	0.522797	67	1600	4187500	152.35	18.71
111 B	1.888339	19710.39	9.323431	2298081	9.01662	0.127256	2.251412	0.008309	2.061159	36.126	2.084982	0.753222	22	900	2444444	105.86	22.68
111 C	1.888117	53245.12	2.394639	3391024	2.253163	0.244967	1.105718	0.015711	1.224026	68.314	1.264491	0.863827	47	900	5222222	119.47	17.49
111 D	1.887896	2209.685	3.136242	2859767	1.19734	0.011684	2.194094	0.000764	2.281632	3.320	2.304018	0.076501	19	3200	593750	276.09	63.66
111 E	1.887674	1581.632	1.915821	2847919	1.091396	0.008421	1.35969	0.000553	1.287998	2.405	1.328001	0.031932	8	2400	333333.3	215.05	76.09
111 F	1.887452	40699.49	2.850952	2973060	1.242122	0.205888	2.152667	0.013588	2.210646	59.106	2.234642	1.320807	38	900	4222222	111.71	18.29
111 G	1.88723	4288.855	3.917496	2847296	1.242537	0.022705	2.88696	0.001488	3.106561	6.472	3.124011	0.202191	29	2500	1160000	276.70	52.10
111 H	1.887008	5412.921	0.883241	2941518	1.108822	0.028628	1.28671	0.001853	1.384104	8.064	1.423573	0.11479	45	6000	750000	145.08	21.73
111 I	1.885012	13319.11	0.709465	3046776	1.526938	0.066538	1.627897	0.004418	1.512918	19.243	1.555645	0.299349	22	900	2444444	197.34	42.18
111 J	1.88479	24384.6	0.794064	2860769	1.391064	0.131025	1.692989	0.008639	1.553363	37.630	1.595766	0.60048	44	2000	2200000	91.57	13.88
111 K	1.884568	24649.03	1.088036	3089882	1.658822	0.125105	1.232686	0.00804	1.295434	35.027	1.346898	0.471783	55	1600	3437500	152.98	20.73
111 L	1.884347	16704.36	2.963776	1985930	1.617623	0.130199	2.460975	0.008416	2.121836	36.666	2.154219	0.789868	32	900	3555556	151.18	26.92
									Sample 1	6.067	2.302	0.139	72.905	98700	1551165	556.02	68.70
										238U Dur	RF	STD	1531			**492.44**	**16.88**
									Sample 2	29.602	1.803	0.504	35.667	23800	1798319	210.17	41.54
										238U Dur	RF	STD	428			**120.46**	**6.17**